Nano Research

Open Access

Review Article

Engineering Ru-based electrocatalysts for efficient electrocatalytic water splitting

Ke Zhang[1], Kang Wang[1], Shimin Chai[1], Luyao Wang[1], Hongying Luo[1], Yanyan Liu[2], Yongfeng Wang[3], Jianchun Jiang[4], and Baojun Li[1]✉

[1] College of Chemistry, Zhengzhou University, Zhengzhou 450001, China
[2] College of Science, Henan Agricultural University, 95 Wenhua Road, Zhengzhou 450002, China
[3] Center for Carbon-based Electronics and Key Laboratory for the Physics and Chemistry of Nanodevices, School of Electronics, Peking University, Beijing 100871, China
[4] Institute of Chemical Industry of Forest Products, Chinese academy of forestry (CAF), National Engineering Lab for Biomass Chemical Utilization, Key and Open Lab on Forest Chemical Engineering, State Forestry Administration (SFA), Nanjing 210042, China

Cite this article: *Nano Research*, **2025**, *18*, 94907369. https://doi.org/10.26599/NR.2025.94907369

ABSTRACT: Electrolysis of water splitting is a clean and sustainable method for hydrogen production without the consumption of fossil fuels or the emission of carbon dioxide. Although a series of non-precious metal catalysts have been developed, they still cannot match the performance of precious metal catalysts in water electrolysis. Ruthenium (Ru), as a noble metal with an ideal cost-to-performance ratio and stable activity, is widely utilized by researchers. However, Ru-sites of electrocatalysts still face several challenges, such as size optimization, structural instability, and electronic structure regulation. This article reviews the design strategies on engineering Ru-based electrocatalysts for efficient water electrolysis, such as atomic-level dispersion, alloying, framework effect, doping, defect engineering, and interface design. And the application progress of precious metal catalysts in the seawater electrolysis was further reviewed and analyzed. These design strategies and their unique advantages provide a valuable theoretical foundation for the future application of Ru-based catalysts in hydrogen production via water electrolysis.

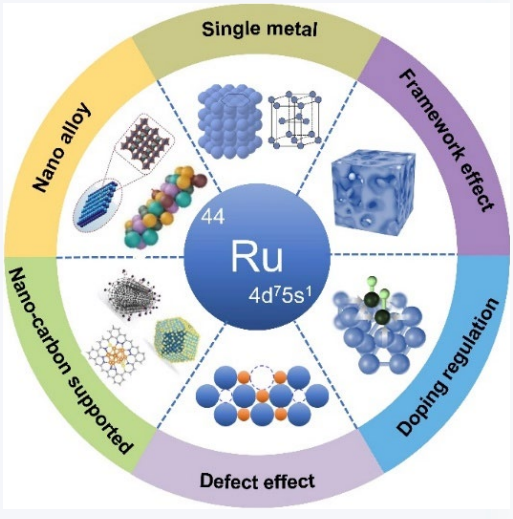

KEYWORDS: Ru catalysts, water electrolysis, framework effect, doping regulation, defect effect, seawater electrolysis

1 Introduction

The global warming effect is becoming increasingly severe due to the rapid advancement of modern industrial processes and the escalating consumption of fossil fuels. The prevailing global consensus now emphasizes green and low-carbon development [1–3]. To address the challenges posed by climate change, over 130 countries and regions worldwide have committed to achieving carbon neutrality, underscoring the unprecedented urgency for accelerated energy transformation [4–8]. Compared with traditional fossil fuels, hydrogen energy represents a novel and promising alternative. It offers several advantages, including zero-carbon emissions, long-term storage capabilities, flexibility, efficiency, and versatile application scenarios [9–13]. To achieve deep decarbonization, it is imperative to expedite the development of hydrogen energy to mitigate climate issues and reduce dependence on fossil fuels, thereby supporting sectors such as transportation, industry, and construction [14–19].

In addition, with the advancement of renewable energy technologies, hydrogen energy is increasingly recognized as a pivotal component of the new power system due to its clean and efficient characteristics [20, 21, 22]. The development of hydrogen energy has garnered significant attention globally, particularly in countries such as China, the United States, Europe, Japan, and South Korea, which have strongly supported research, development, and innovation in this field [23–26]. Currently, the global push toward "carbon neutrality" has elevated the development of the hydrogen industry as a key strategy for

Received: January 24, 2025; **Revised:** March 8, 2025
Accepted: March 14, 2025

✉Address correspondence to lbjfcl@zzu.edu.cn

addressing climate change, making it a critical development goal for many major countries and regions [27] . Simultaneously, resolving challenges related to hydrogen production, distribution, transportation, and storage is essential for establishing a hydrogen economy and supporting strategic initiatives (see Fig. 1 from Ref. [28]) Among these issues, hydrogen production stands out as the most pressing concern.

Methanol decomposition [29–33], ammonia disintegration [34–37], biomass conversion [38–40], photocatalytic water splitting [41, 42], and electrochemical hydrolysis are currently the primary technologies for large-scale hydrogen production. Methanol decomposition produces CO_2, while ammonia disintegration yields N_2, both of which require further purification. Among these hydrogen production methods, biomass and photocatalytic hydrogen generation suffer from low technical efficiency and complex processes, making them less competitive compared to electrochemical water splitting. Electrochemical water decomposition is presently one of the most ideal hydrogen production techniques due to its ability to achieve up to 99.9% hydrogen purity in electrolytic water reactions [43]. However, the catalytic mechanisms for anodic and cathodic polarization differ significantly. Catalysts with high activity for the hydrogen evolution reaction (HER) do not necessarily exhibit high activity for the oxygen evolution reaction (OER), and vice versa. Currently, researchers predominantly use metals as electrolytic hydrolysis catalysts. Suitable metals and non-metallic elements for hydrolysis are illustrated in (see Fig. 2 from Ref. [44]). Both precious and non-precious metal catalysts have been extensively studied as effective electrolytic water catalysts. Non-precious metals such as Fe and Co offer advantages in terms of low cost and high abundance but exhibit lower catalytic activity, limiting their practical application. Precious metal catalysts like Pt and Ru possess excellent catalytic activity but are constrained by high costs and limited availability. These catalysts are currently recognized as the most ideal electrolytic water catalysts. However, the high cost of precious metal catalysts hinders further development in this area [45–50]. Therefore, reducing costs while ensuring catalytic activity remains a key research focus. For instance, certain transition metals, such as those similar to Pt but with lower costs and higher catalytic activity than non-precious metals, represent promising research goals [51–55].

It is evident that electrocatalytic water splitting represents a carbon-free and environmentally sustainable route for hydrogen production. Despite the continued preference for precious metals as electrocatalysts, the design and development of these catalysts remain a critical factor limiting their practical application. While Pt-based catalysts exhibit superior catalytic performance, their high cost has led to increased attention on Ru-based catalysts, which possess a similar d-band electronic structure but at a relatively lower price. However, advancing Ru-based electrocatalysts necessitates addressing the challenges of designing unique catalyst morphologies and optimizing the electronic structure of Ru sites. Consequently, it is imperative to synthesize theoretical design principles of Ru-based catalysts and establish structure-activity relationship models from extensive research literature. This review begins by examining the mechanism of electrocatalytic water splitting across varying pH environments, systematically analyzing and summarizing the progress in precious metal catalysts for electrocatalytic water splitting over the past five years. It further highlights the research advancements and key challenges faced by Ru-based catalysts, along with corresponding improvement strategies. Additionally, this review elucidates the distinctive advantages of engineering Ru-based catalyst design, providing a robust theoretical foundation for optimizing the structure-activity relationship and developing Ru-based catalysts with enhanced electrocatalytic water splitting performance.

2 Principles and challenges in water electrolysis

2.1 Principles of water electrolysis

By leveraging advancements in renewable energy sources like wind, solar, and tidal power, water electrolysis has emerged as a promising method for producing high-purity hydrogen [56–61]. This hydrogen can be utilized efficiently for energy storage and

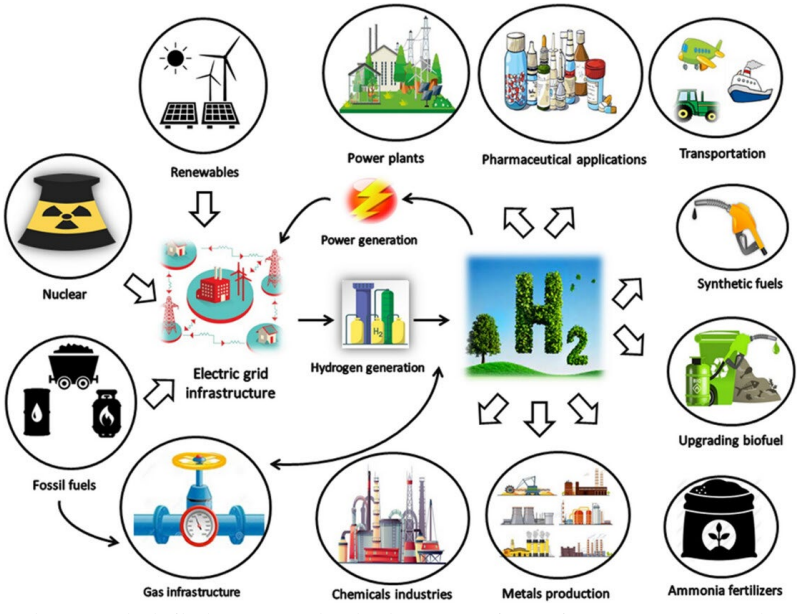

Figure 1 The manufacturing and application method of hydrogen. Reproduced with permission from Ref. [28], © Osman, A. I. et al. 2021.

conversion purposes [62–68]. The fundamental reaction in water electrolysis is the decomposition of water into hydrogen gas at the cathode and oxygen gas at the anode, summarized by the equation $2H_2O \rightarrow 2H_2 + O_2$ [69–75] (see Fig. 3 adapted from Ref. [56]). The HER varies in its mechanism depending on the acidity or alkalinity of the electrolyte, with multiple steps involved in the reaction process. Additionally, the OER plays a crucial role in water electrolysis. The detailed reaction mechanism of water electrolysis is outlined below.

Figure 2 The type of scarce element and its potential application as a hydrolyzed electric catalyst. Reproduced with permission from Ref. [44], © Elsevier B.V. 2021. All rights reserved.

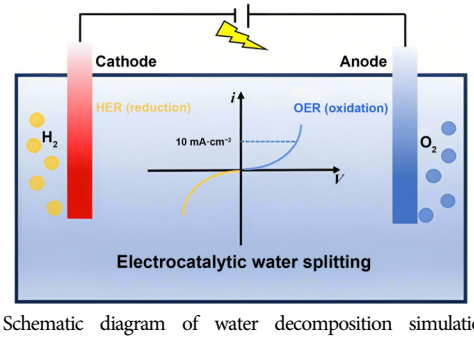

Figure 3 Schematic diagram of water decomposition simulation device. Adapted with permission from Ref. [56], © Wiley-VCH GmbH 2023.

In acidic electrolytes, the reactions at the electrodes during water electrolysis are as follows (Eqs. (1) and (2))

$$\text{At the cathode: } 4H^+ + 4e^- \rightarrow 2H_2 \quad (1)$$

$$\text{At the anode: } 2H_2O \rightarrow 4H^+ + O_2 + 4e^- \quad (2)$$

For alkaline or neutral electrolytes, the electrode reactions are Eqs. (3) and (4)

$$\text{At the anode: } 4OH^- \rightarrow 2H_2O + O_2 + 4e^- \quad (3)$$

$$\text{At the cathode: } 4H_2O + 4e^- \rightarrow 2H_2 + 4OH^- \quad (4)$$

Since the first report of water decomposition in 1789, the history of water electrolysis has spanned over two centuries [55] . With the continuous advancement of electrolytic water technology, electrocatalysts have gradually found applications in industry. The first commercial electrolyzer was introduced in 1948. In the 21st century, with growing concerns about environmental pollution and energy challenges, hydrogen has gained widespread attention for research and application [76, 77] (see Fig. 4 adapted from Ref. [76]). Water decomposition involves two key half-reactions: HER and OER. The OER, which involves a slower four-electron transfer process, presents greater challenges compared to the HER. Historically, catalysts based on platinum (Pt), iridium (Ir), and ruthenium [Ru] have been favored for their superior performance in both HER and OER. However, the high cost and limited availability of these precious metals have hindered their widespread adoption. Consequently, there is a pressing need to develop low-cost catalysts that can match the efficiency of Pt-based materials for water splitting [76].

2.1.1 *HER mechanism*

HER entails the transfer of two electrons at the cathode. Depending on the chemical environment provided by electrolytes under different pH conditions, HER demonstrates distinct behaviors in acidic, neutral, and alkaline media. From a kinetic standpoint, H_2 production can proceed via two primary pathways: the Volmer–Heyrovsky and the Volmer–Tafel mechanisms. As shown in figure (see Fig. 5 adapted from Ref. [78]), during the Volmer step, an adsorbed hydrogen intermediate (*H), where * denotes the active intermediate on the electrode surface, is formed through the

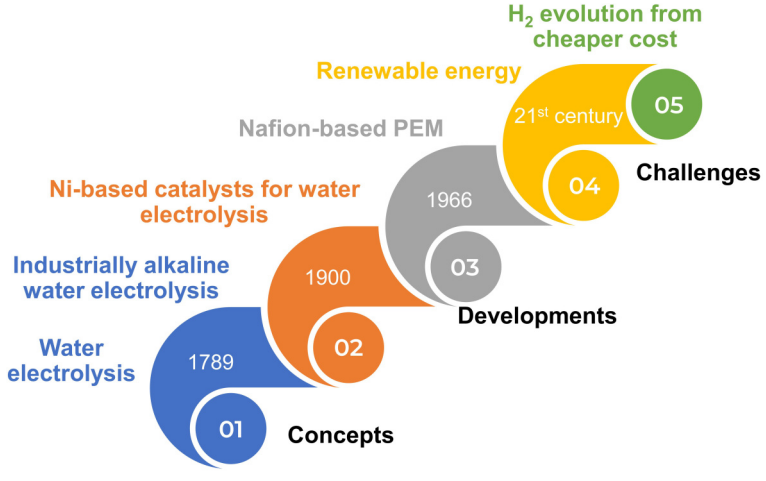

Figure 4 The development history of electrolytic water catalysts. Adapted with permission from Ref. [76], © Wiley-VCH GmbH 2021.

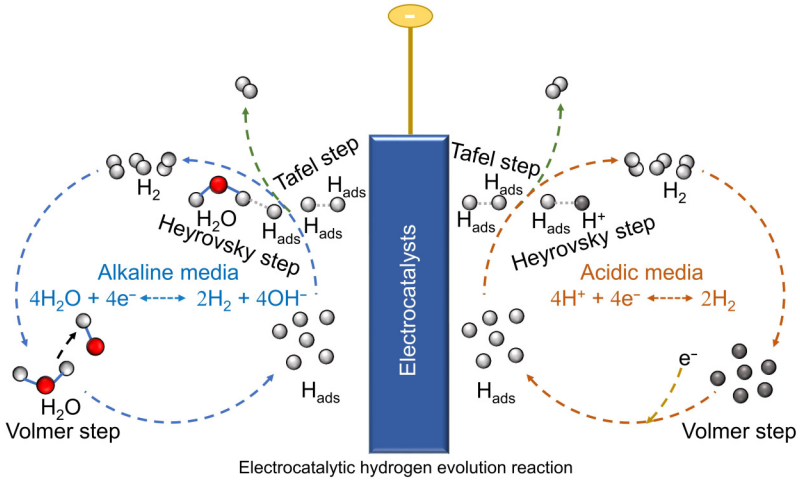

Figure 5 Two reaction mechanisms of HER under acidic and alkaline conditions. Adapted with permission from Ref. [78], © Kazemi, A. et al. 2024. Published by American Chemical Society.

combination of hydronium ions (H_3O^+) and electrons (e^-) on the surface of acidic electrolytes [78, 79].

In an alkaline environment, it is difficult for H_2O molecules to directly react in the solution. Instead, water molecules first adsorb onto the catalyst surface, where they acquire electrons (e^-) to form *H (an active intermediate) and OH^- ions. During the Heyrovsky step, *H can combine with either H_3O^+ or H_2O to produce H_2. Alternatively, during the Tafel step, two *H intermediates can combine to directly release H_2. The HER mechanism of the catalyst can be evaluated using the catalytic Tafel slope, a key kinetic parameter for assessing electrocatalyst activity. The HER process involves multiple steps, each contributing to the overall reaction kinetics [80]. The specific steps of HER are outlined as following formulae (Eqs. (5)–(9))

Volmer reaction:

$$H^+ + e^- + M \rightarrow MH_{ads} \quad \text{(acidic electrolyte)} \tag{5}$$

$$H_2O + M + e^- \rightarrow MH_{ads} + OH^- \quad \text{(alkaline electrolyte)} \tag{6}$$

Heyrovsky reaction:

$$MH_{ads} + H^+ + e^- \rightarrow M + H_2 \quad \text{(acidic electrolyte:)} \tag{7}$$

$$H_2O + e^- + MH_{ads} \rightarrow H_2 \quad \text{(alkaline electrolyte)} \tag{8}$$

Tafel reaction:

$$2MH_{ads} \rightarrow H_2 + 2M \quad \text{(acidic and alkaline electrolyte)} \tag{9}$$

HER process highlights that the key rate-determining steps in electrocatalytic hydrogen generation are significantly influenced by the strength of adsorption between intermediates and the catalyst surface. When the catalyst exhibits weak binding with *H, this step limits the HER process. Conversely, if the adsorption between the catalyst and *H is too strong, it hinders the release of H_2, making the desorption step the rate-limiting factor. The adsorption free energy of hydrogen ($\Delta G(H^*)$) serves as a crucial descriptor for evaluating catalytic activity. This parameter can be calculated using density functional theory (DFT). Ideally, for optimal catalytic performance, $\Delta G(H^*)$ should approach zero [81].

2.1.2 *OER mechanism*

The OER is the other half of water decomposition and is more complex than the HER. The OER process involves the transfer of multiple electrons and protons. The reaction pathway of OER varies depending on the type of electrolyte [82, 83] . As shown in Figure (see Fig. 6 in Ref. [83]), in both alkaline and acidic electrolytes, intermediates such as *OH, *O, and *OOH are continuously formed. The differences caused by varying pH levels are primarily due to different concentrations of reactants (H^+ or OH^-). In acidic media, the additional water dissociation step results in a slower formation rate of *OH and *OOH compared to that in alkaline media. Consequently, the intermediate products formed at each step directly influence catalytic efficiency. Similar to the binding energy of hydrogen during HER, the interaction between the electrocatalyst and intermediates is critical for enhancing the catalytic activity of electrocatalysts in the OER process [75, 84–89].

The response mechanism of acidic electrolyte is Eqs. (10)–(14)

$$M^* + H_2O \rightarrow MOH^* + H^+ + e^- \tag{10}$$

$$MOH^* \rightarrow MO^* \rightarrow + H^+ + e^- \tag{11}$$

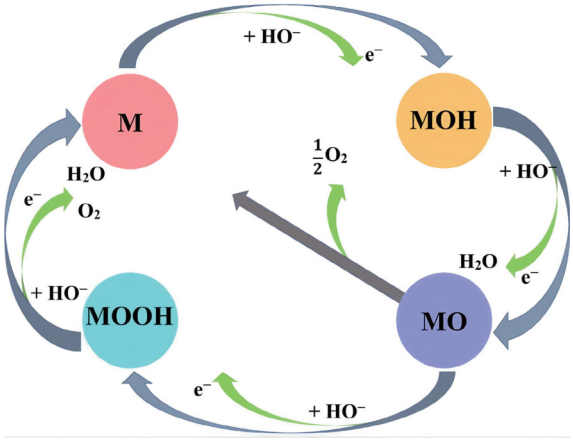

Figure 6 The response mechanism of OER in acidic and alkaline conditions. Reproduced with permission from Ref. [83], © American Chemical Society 2020.

$$MO^* + H_2O \rightarrow MOOH^* + H^+ + e^- \quad (12)$$

$$MOOH^* \rightarrow MO_2^* + H^+ + e^- \quad (13)$$

$$MO_2^* \rightarrow M + O_2 \quad (14)$$

The specific reaction mechanism of alkaline electrolyte is as follows (Eqs. (15)–(19))

$$OH^- + M^* \rightarrow MOH^* + e^- \quad (15)$$

$$MOH^* + OH^- \rightarrow MO^* + H_2O + e^- \quad (16)$$

$$MO^* + OH^- \rightarrow M^*OOH + e^- \quad (17)$$

$$M^*OOH + OH^- \rightarrow M^* + O_2 + H_2O + e^- \quad (18)$$

$$2MO^* \rightarrow 2M^* + O_2 \quad (19)$$

In an alkaline environment, OER typically proceeds through the following mechanism. Initially, the catalytic active site (M*) binds with a hydroxyl ion (OH^-) to form an MOH* intermediate. This MOH* intermediate then reacts with another OH^- to produce an MO* species [90–94]. The MO* intermediate subsequently interacts with an additional OH^- to form an M*OOH intermediate. Finally, the M*OOH intermediate combines with one more hydroxyl group to release oxygen molecules. Each of the four steps in the OER process is associated with an energy barrier, and the highest of these barriers determines the rate-limiting step. Therefore, the overall difficulty of the reaction is dictated by this highest energy barrier.

2.2 Challenges of water electrolysis

In the process of water electrolysis, both HER and OER exhibit high reaction energies. Consequently, the actual voltage required is greater than the theoretical starting voltage of 1.23 V. The efficiency and cost of hydrogen production are highly dependent on the choice of catalysts [95–97]. The pH of the electrolyte also significantly impacts catalyst research. In acidic media, water decomposition requires stable, rare, expensive, and acid-insoluble catalysts. Therefore, developing effective, economical, and abundant HER catalysts in neutral or alkaline media is crucial for improving overall hydrolysis efficiency and enhancing dual-functional electrocatalysts for OER. Although non-precious metal catalysts are economically viable and abundant, they exhibit lower catalytic activity compared to precious metal catalysts, which are used under alkaline conditions due to their superior catalytic performance [98–103]. Consequently, scientists continue to investigate high-performance, high-activity, and cost-effective precious metal catalysts [104, 105]. However, due to their high cost and limited availability, the widespread application of precious metal catalysts remains constrained, limiting large-scale development of water electrolysis. To reduce costs while maintaining and enhancing catalytic activity, researchers are actively pursuing the development of more ideal electrolytic water catalysts. These advancements are vital for the practical application of energy storage and conversion technologies [106–108].

3 Research status of electrocatalysts

Because most electrocatalysts demonstrate high activity primarily in either the HER or the OER, but not both, the overall efficiency of electrolysis systems is constrained, thereby impeding the advancement of electrolytic water devices. Consequently, there is an urgent need to develop high-efficiency, highly active, and stable dual-functional catalysts that can excel in both HER and OER. Given the rigorous conditions encountered in practical water electrolysis, achieving and maintaining high activity and long-term stability in these systems remains a significant challenge. The development of such dual-functional catalysts is crucial for enhancing the performance and reliability of electrolysis technologies. Under these conditions, precious metal catalysts are currently the only ones capable of meeting long-term stable operation requirements due to their superior catalytic activity, excellent stability, and controllable structures [96, 97]. However, current research on precious metal catalysts is insufficient, necessitating continued efforts from researchers to innovate and improve these catalysts. Key directions for developing high-efficiency, durable, and economical electrolytic water catalysts include reducing the loading of precious metals, enhancing precious metal utilization, and extending catalyst lifespan [96, 109–114].

3.1 Research progress of precious metal catalysts

High-performance catalyst materials have consistently been a focal point for researchers, who have made significant efforts in this area. A three-dimensional nanoporous Ni-Mo electrocatalyst exhibits minimal overpotential for alkaline hydrogen evolution [98, 104, 105]. The advantages of precious metal catalysts include: (1) their high intrinsic activity, characterized by optimal intermediate adsorption/desorption energies; and (2) their stability across the entire pH range. Consequently, precious metal-based catalysts are considered the optimal choice for electrolysis applications. Researchers have developed various types of precious metal catalysts, laying a solid foundation for further advancements in this field (see Fig. 7 adapted from Ref. [56]).

The volcano plot is a graphical representation derived from DFT calculations of metal materials, used to compare their catalytic activities. Typically, the peak of the volcano plot indicates the highest catalytic activity for a given catalyst. As shown in Fig. 8, the highest HER activity is exhibited by Pt, while the most active OER catalysts are metal oxides such as Ir, Ru, and cobalt (Co). Pt often referred to as a "star" catalyst [106, 115–118]. These catalyst have been extensively studied; however, its low abundance and high cost have significantly limited the further development of Pt-based catalysts [106, 107, 119–121]. Ru, which belongs to the same group as Pt [122, 123], costs only about one-quarter as much as Pt and shares similar properties. As a result, Ru-based catalysts have emerged as promising candidates. Researchers are actively focusing on improving the catalytic performance of these Ru-based materials.

3.2 Research status of Ru-based catalysts

Ru is less costly than precious metals such as Pt and Ir and is more stable compared to non-precious metals. Therefore, Ru-based catalysts have become a high-quality choice for bifunctional electrocatalytic water decomposition. However, Ru-sites in electrocatalysts face a number of challenges that limit their practical application. These challenges include structural instability under long-term operation, strong adsorption of reaction intermediates

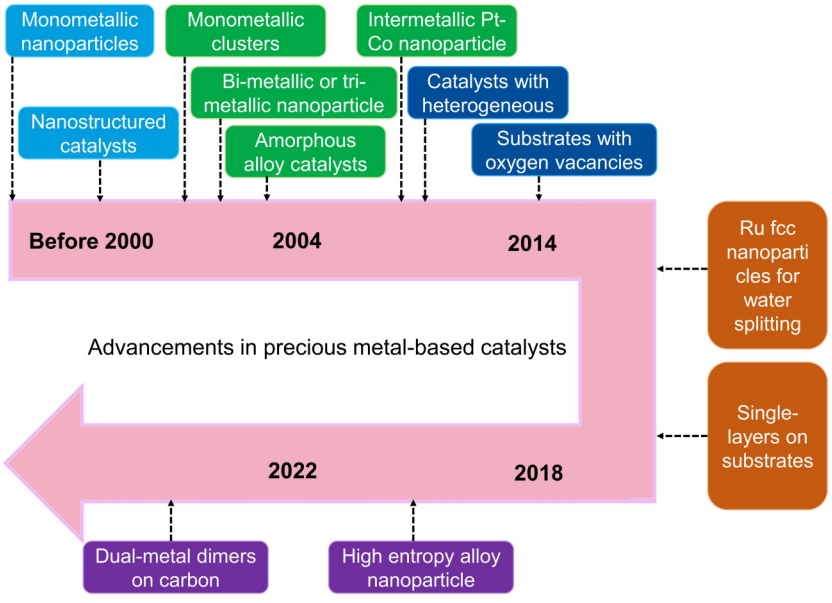

Figure 7 Development of precious metal catalysts. Adapted with permission from Ref. [56], © Wiley-VCH Verlag GmbH & Co. KGaA, Weinheim 2019.

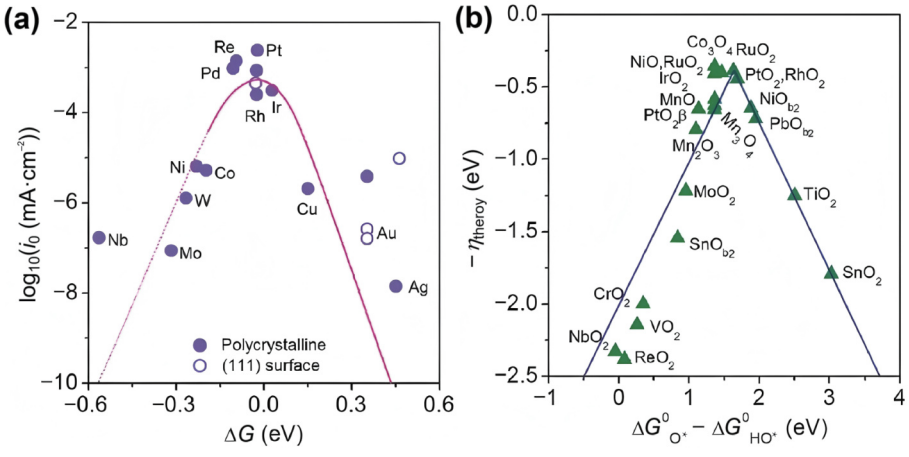

Figure 8 (a)The relationship between the Gibbs free energy of hydrogen binding on various metal surfaces and their hydrogen production activity. Circles are experimental data, and the curve is from microkinetic theory. Reproduced with permission from Ref. [106], © American Chemical Society 2010. (b) The correlation of OH* and OOH* adsorption energies on different catalysts surfaces during oxygen evolution reactions (OER). Reproduced with permission from Ref. [115], © WILEY-VCH Verlag GmbH & Co. KGaA, Weinheim 2011.

leading to catalyst poisoning, and the need for further optimization of the electronic properties to improve activity and durability. Addressing these challenges is essential to realize the full potential of Ru-based catalysts for sustainable energy applications. Atomic engineering of Ru-based catalysts, including atomic composition, coordination microenvironments and structural design, is essential for optimizing reaction pathways and improving Ru utilization [124]. The problems faced by ruthenium sites can be solved by changing the atomic composition, coordination microenvironment and structural design of the catalyst. For example, the stability of the catalysts can be improved by structural design, compositing of ruthenium with carriers (carbon carriers, etc.), and the toxicity of the catalysts can be solved by means of coordination microenvironments, alloying of ruthenium with other metals, or doping with heteroatoms, which are helpful for improving the activity and durability of the catalysts. In this paper, the catalytic advantages of ruthenium-based catalysts and their modulation strategies will be illustrated from the following aspects: firstly, the crystal phase modulation of ruthenium-based monometallic catalysts; secondly, the alloying effect of ruthenium alloyed catalysts; and thirdly, the size effect and matrix effect of ruthenium-based composite catalysts (see Scheme 1 adapted from Ref. [56]). Among them, the monatomic catalysts in ruthenium-based monometallic catalysts have attracted much attention from researchers due to their extremely high atomic utilization. Therefore, this paper will focus on Ru-based single metal catalysts, Ru alloy catalysts and Ru-based composite catalysts. In addition, the industrial applications of ruthenium-based catalysts will be explored, as well as their potential application in the field of electrolysis of seawater.

3.2.1 *Recent advances in Ru-sites of electrocatalysts*

Recent studies have demonstrated the significant impact of structural modifications on the performance of Ru-sites in electrocatalysts. For example, Ru NPs was encapsulated in nitrogen-doped graphite carbon foam (Ru-NGC) by pyrolysis [125]. The result presented that a small amount of Ru NPs was surrounded by several layers of nitrogen-doped graphitized carbon shells with an interlayer distance of 0.34 nm. The catalyst exhibited good HER

performance and stability owing to the uniform distribution of Ru NPs and the protection of the graphite layer. Ru-NGC shows a similar overpotential (25 vs. 29 mV) and Tafel slope (31 vs. 29 mV·dec^{-1}) to Pt/C at a current density of 10 mA·cm^{-2} in 0.5 M H_2SO_4. Graphene support derived from graphite is also an excellent choice as catalyst support. Similarly, Ru nanoparticles embedded in a metal-organic framework (MOF) showed excellent OER performance, with an overpotential of 230 mV at 10 mA·cm^{-2} [126]. The porous structure of the MOF facilitated mass transfer and provided abundant active sites, contributing to the high catalytic activity. These findings underscore the importance of structural engineering in optimizing the performance of Ru-sites in electrocatalysts.

3.2.2 *Stability challenges and improvement strategies*

The instability of Ru-sites in electrocatalysts is a critical issue that affects their practical application. Long-term operation often leads to catalyst degradation, agglomeration of Ru nanoparticles, and poisoning by reaction intermediates. For instance, Li et al. [127] reported that Ru-based catalysts exhibited significant performance decline after prolonged cycling due to the strong adsorption of hydroxyl groups (*OH) on Ru-sites, which hindered hydrogen evolution.

To address these challenges, several strategies have been proposed. One effective approach is the use of supports with high conductivity and stability, such as nitrogen-doped carbon, which can enhance electron transfer and prevent Ru agglomeration. Liu et al. [128] prepared vacancy-rich carbon dots (CDs) supported Ru nanoparticles (Ru@CDs) via two-step pyrolysis strategy. The abundant vacancies and functional groups (such as NH_2, COOH, OH) in CDs provided favorable binding sites for Ru nanoparticles, which could effectively prevent the aggregation of Ru. The obtained Ru@CDs exhibited a small size of 5 nm and only required an overpotential of 30 mV at 10 mA·cm^{-2} in 1.0 M KOH. Spectroscopic characterizations and DFT calculations indicated that the abundant vacancies and strong electronic interactions between CDs and Ru could promote water dissociation and regulate hydrogen adsorption/desorption, thereby synergistically promoting HER catalytic activity. Another strategy involves the incorporation of stabilizing elements or the design of core-shell structures to protect Ru-sites from degradation. Che et al. [129] reported a series of hollow carbon sphere supported Ru nanoparticles. It is demonstrated that the nucleation, growth, and fixation process of the Ru nanoparticles could be readily controlled by adjusting the ligands, which could lead to Ru NPs with different sizes and dispersions. The smaller Ru cluster exhibited higher HER catalytic activity due to the quantum size effect, more electrochemically active sites, optimized surface H adsorption capacity and higher intrinsic activity. Especially, the ultra-small Ru nanoparticles with mean size of 1.5 nm exhibited a small overpotential of 31 mV at 10 mA·cm^{-2}, a low Tafel slope of 26 mV·dec^{-1}, and a large exchange current density of 1.7 mA·cm^{-2}.

In another work, a ultra-small ruthenium nanoparticles was confined in hollow nitrogen-doped carbon spheres (Ru/HNCS) by pyrolyzing Ru^{3+} coordinated dopamine coated SiO_2 sphere [130]. Even though the Ru content is less than 0.1 wt.%, Ru/HNCS still exhibited excellent HER activity, and a small overpotential of 39 mV was achieved at 10 mA·cm^{-2}. This good performance could be attributed to the strong coupling of ultra-small Ru nanoparticles and the highly dispersed active sites, as well as the synergistic effect between noble metal and hollow carbon sphere support.

These measures have demonstrated significant improvements in enhancing the stability of ruthenium-based electrocatalysts, thereby facilitating their practical application in large-scale water electrolysis.

3.2.3 *Industrial applications of Ru-sites in electrocatalysts*

The application of Ru-sites in electrocatalysts for industrial processes, particularly seawater electrolysis, presents both opportunities and challenges. Seawater electrolysis is a promising method for large-scale hydrogen production; however, the complex chemical environment of seawater poses significant challenges to catalyst stability and activity.

Recent studies have shown that Ru-based catalysts can achieve high performance in seawater electrolysis. For instance, Kang et al. [131] developed a RuMoNi catalyst that demonstrated excellent stability and activity in alkaline seawater electrolytes. Nevertheless, challenges such as chloride-induced corrosion and the competitive

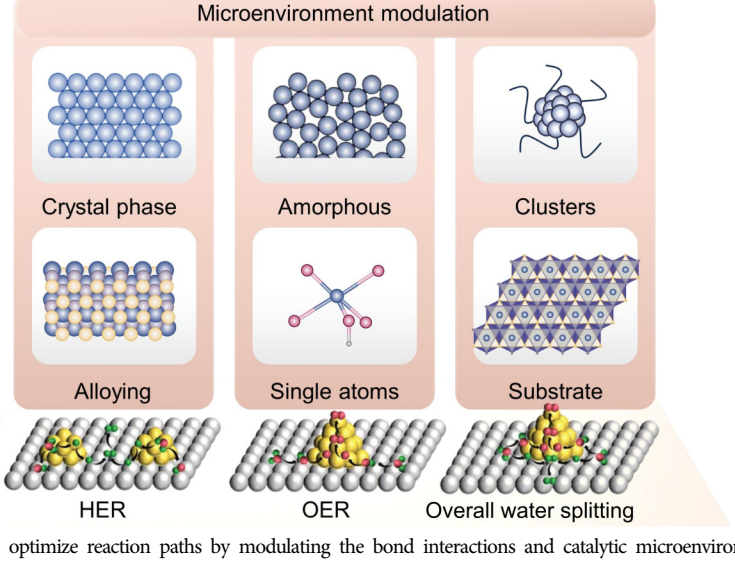

Scheme 1 Typical design strategies to optimize reaction paths by modulating the bond interactions and catalytic microenvironments in noble metals-engineered catalysts. Adapted from Ref. [56], © Wiley-VCH GmbH 2023.

chlorine oxidation reaction (ClOR) remain formidable hurdles.

Future research should concentrate on optimizing Ru-sites through advanced synthesis strategies, including defect engineering and heteroatom doping, to enhance stability and activity. Additionally, investigating deactivation mechanisms and developing protective coatings can further improve the long-term performance of Ru-based catalysts in industrial applications.

3.3 Synthesis strategies for Ru-sites of electrocatalysts

3.3.1 Single metal Ru-based catalysts

Single-metal Ru-based catalysts involve the discussion of the crystal phase of the catalyst. By adjusting the atomic arrangement of the metal, the electronic structure and chemical state can be designed on the atomic scale [126]. Different atomic arrangements of single metals exhibit distinct crystal phases, and thus, regulating the crystal phase can effectively alter their intrinsic properties [132].

Recently, researchers have been actively investigating various crystal phases of rationally designed single-metal catalysts. Among these metals, Rh, Pd, Ir, and Pt predominantly adopt a face-centered cubic (fcc) structure, while Ru and Os favor a hexagonal close-packed (hcp) structure (see Fig. 9(a) from Ref. [133]). In the fcc structure, the stacking sequence follows an ABC pattern, whereas in the hcp structure, it is AB (Fig. 9(b)). These structures are referred to as 3C for fcc and 2H for hcp. For hexagonal structures, longer stacking cycles can occur along the (100) direction, such as ABCB (4H structure) [133, 136–140]. Different crystal structures typically exhibit varying catalytic activities due to their distinct electronic coordination sites. Zhang's team explored the influence of crystal structure on HER catalyst performance using synthesized Ru-based catalysts with different crystal structures. Transmission electron microscopy (TEM) images revealed both fcc and hcp structures for Ru (see Fig. 9(c) from Ref. [134]). DFT calculations indicated that the fcc structure of Ru outperforms the hcp structure in optimizing H adsorption energy and reducing water dissociation energy (see Fig. 9(d) from Ref. [134]). In addition, Ru-based catalysts exhibit excellent OER activity compared to commercial Pt/C catalysts. Zhao and his team designed Ru octahedral

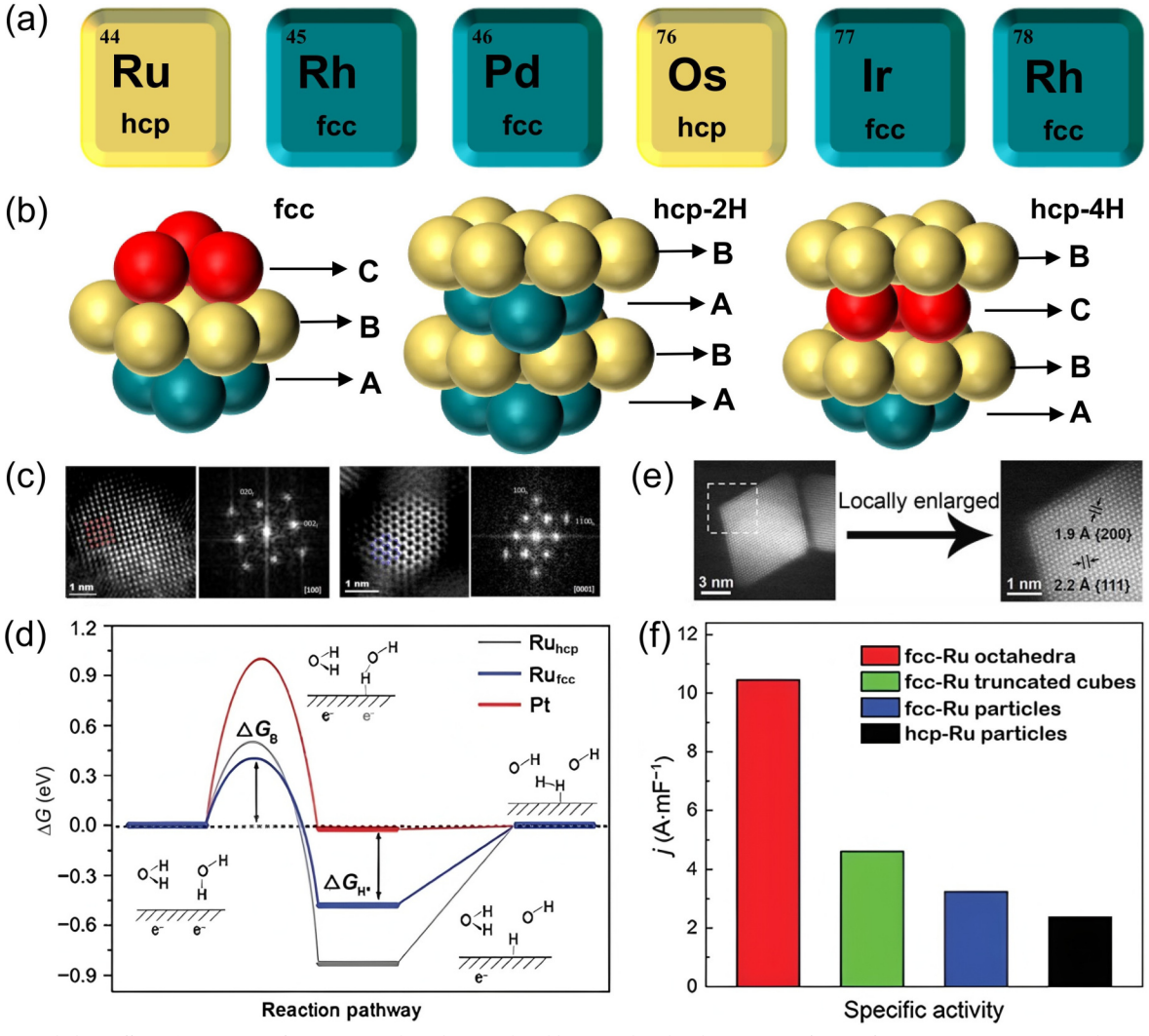

Figure 9 Crystal phase effect. (a) A portion of precious metals in the periodic table. Reproduced with permission from Ref. [133], @ WILEY-VCH Verlag GmbH & Co. KGaA, Weinheim 2018. (b) Crystal face diagrams in fcc, hcp-2H, and -4H structures, (c) high-angle toroidal dark-field scanning transmission electron microscopy (HAADF-STEM) images of Ru nanoparticles showing fcc and fcc/hcp and their corresponding adsorption energies, (d) Gibbs free energy diagram of HER on Pt/Ru surface. Reproduced with permission from Ref. [134], @ American Chemical Society 2016. (e) TEM images of Ru octahedral crystals and (f) activity ratios of different Ru based catalysts. Reproduced with permission from Ref. [135], @ American Chemical Society 2019.

nanocrystals with an fcc structure instead of the traditional hcp lattice. The final product featured an octahedral shape surrounded by Ru(111) crystal facets (see Fig. 9(e) from Ref. [135]). In OER, the overpotential of Ru octahedral nanocrystals was lower than that of Ru with an hcp structure, demonstrating activity 4.4 times higher (see Fig. 9(f) from Ref. [135]). Therefore, under certain conditions, the Ru(111) crystal surface exhibits superior catalytic activity compared to the Ru(100) surface, although the specific mechanism remains unclear.

In summary, the crystal structure and crystal facets of Ru can be considered an effective method to enhance its catalytic performance. However, challenges remain in obtaining new crystal phases in Ru-based catalysts with fine nanostructures and active sites. Despite these challenges, research on Ru crystal structures and surfaces has laid a foundation for further elucidating the reaction mechanisms of Ru as a catalyst. Additionally, Ru-based alloy catalysts, which form alloys with other precious or non-precious metals, exhibit synergistic effects and participate in electrolytic water catalysis.

3.3.2 *Single-atom Ru-based catalysts*

Single-atom catalysts have garnered significant attention due to their unique properties and potential for high catalytic performance. In the context of Ru-based catalysts, single-atom Ru catalysts offer several advantages, including maximized atom utilization and tunable electronic properties. These catalysts can be designed to optimize the adsorption and desorption energies of reaction intermediates, thereby enhancing the overall catalytic efficiency.

Recent studies have demonstrated the potential of single-atom Ru catalysts in both acidic and alkaline media. For example, a study reported the synthesis of Ru single atoms supported on nitrogen-doped carbon, which exhibited excellent HER performance across a wide pH range [141]. The high dispersion of Ru atoms and the strong interaction with the nitrogen-doped support were found to significantly enhance the catalytic activity and stability.

The potential applications of single-atom Ru catalysts extend beyond HER to include OER and overall water splitting [142]. By optimizing the electronic structure of Ru atoms through support engineering, these catalysts can achieve high activity and selectivity in various electrochemical reactions. Future research should focus on developing scalable synthesis methods and exploring new support materials to further enhance the performance of single-atom Ru catalysts.

3.3.3 *Ru-based alloy catalysts*

Interactions between metals can lead to changes in the electronic structure due to electronic transmission between different atomic components [143–145]. The varying electronic structures of different metals result in differences in chemical reactions [146]. Therefore, forming alloys with Ru can adjust its electronic structure, increase active sites, and reduce the content of precious metals, thereby enhancing the utilization rate of precious metals [147, 148]. Consequently, designing Ru-doped alloys is an effective strategy for developing Ru-based catalysts [149, 150]. Currently, Ru alloy catalysts include binary metal alloys, ternary metal alloys, and high-entropy alloys (HEAs). These alloy catalysts have demonstrated excellent performance in various catalytic reactions [151, 152].

For example, Mu's group investigated $RuRh_2$ bimetallic alloy catalysts with a high density of defect structures and active sites [153]. They found that the incorporation of Rh enhanced electron transport and reactant adsorption, while also modulating the strong adsorption of Ru to *H. The experimental results demonstrated that the linear sweep voltammetry (LSV) curve of the catalyst remained virtually unchanged after 20,000 CV cycles, indicating excellent stability. The alloying is also an effective strategy to enhance catalytic activity. Ho's group developed an approach by synthesizing the $RuIrO_x$ alloy catalyst through incorporating Ru into IrO_x (see Figs. 10(a)–10(c) from Ref. [154]). By forming alloys, the Fermi levels of Ru and IrO_x were adjusted, thereby improving the catalyst's activity [154].

In addition to binary metal alloys, Ru-based catalysts can also be alloyed with various non-precious metals, such as PtRuFe and RuCoMo alloys [155], thereby enhancing catalytic performance while reducing catalyst costs [156]. The development of HEAs has gradually revealed their excellent catalytic properties. By synthesizing HEAs with diverse atomic configurations, such as FeCoNiXRu (where X can be Cu, Cr, or Mn), the alloy system demonstrates varying adsorption capabilities for different intermediates (see Fig. 10(d) from Ref. [157]). The presence of the fifth metal (X: Cu, Cr, Mn) introduces unique characteristics that facilitate charge transfer within the FeCoNiXRu alloy, resulting in distinct patterns of charge redistribution. Partial density of states (PDOS) analysis reveals that the Ru active center in FeCoNiMnRu exhibits a higher electron density, with charge transferring from other transition metals to Ru (see Fig. 10(e) from Ref. [157]). Recent Raman spectroscopy studies have shown that Fe, Co, Ni, Ru, and X (Cu, Cr, Mn) each play distinct roles in HER. Specifically, during the reaction process, Ru forms Ru–H bonds (see Fig. 10(f) from Ref. [157]). The FeCoNiMnRu HEA features four distinct atomic configurations at its catalytic sites (see Fig. 10(g) from Ref. [157]), and the synergy between these active sites significantly enhances catalytic activity. Compared to binary and ternary metal alloys, HEAs provide a broader range of active sites, which is crucial for the development and design of multifunctional catalysts. This diversity in active sites offers greater flexibility and potential for optimizing catalytic performance across various applications [158, 159].

3.3.4 *Ru-coupled carbon nanocatalysts*

Carbon is an excellent conductive material. By modifying carbon materials, one can alter the coordination and interaction of key active sites. When compounded with precious metals, such modifications can stabilize metal active sites, thereby enhancing catalyst activity and stability [160]. The high utilization rate of the catalyst is achieved through this approach. Additionally, when using heteroatom-doped carbon materials, the interaction between the modified carbon and metal further improves catalytic performance.

The catalytic corrosion resistance and stability are crucial factors for the practical application of catalysts. To develop high-efficiency and long-lasting Ru-based electrocatalysts for water electrolysis, researchers often combine ruthenium with low-cost, high-surface-area, and highly conductive carbon materials as a support. This approach enhances catalyst performance by optimizing the electronic structure of Ru, thereby improving its catalytic activity [161–163]. The Ru-carbon composites expose more active sites, facilitating electron transfer and modulating the electronic distribution of Ru, which further enhances catalytic performance [141].

Three design strategies for carbon-based catalysts:

Recent studies have explored the development of Ru-based

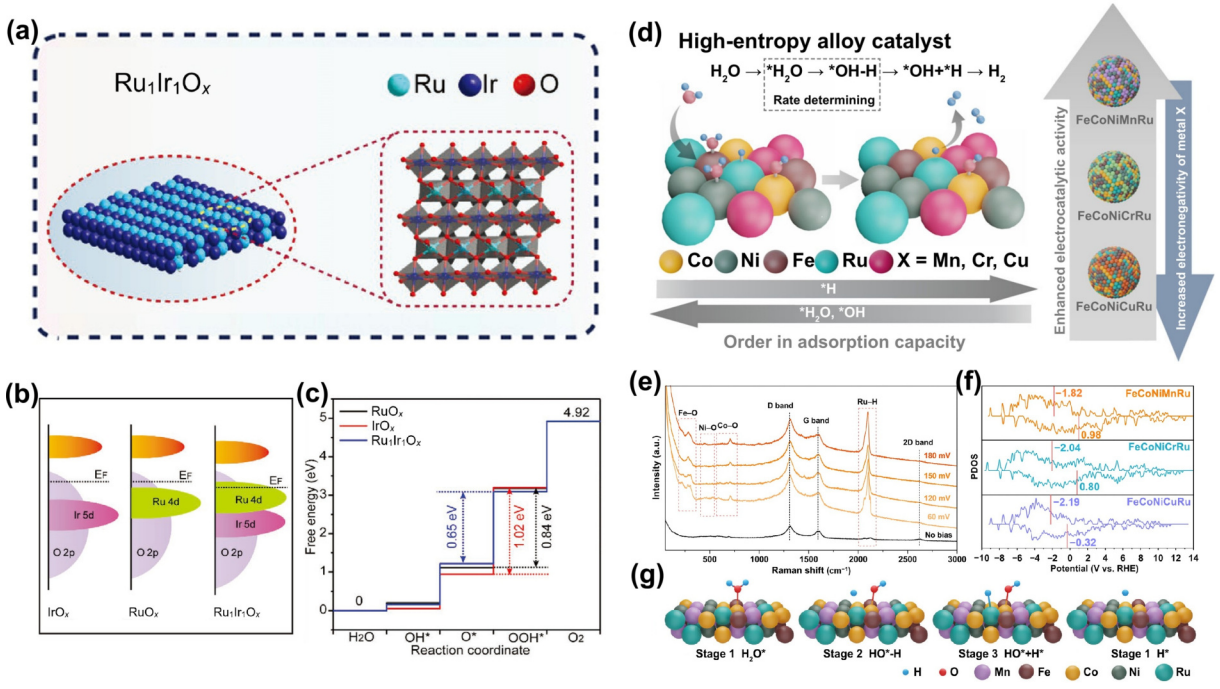

Figure 10 (a) The schematic diagram of the $Ru_1Ir_1O_x$, (b) the energy band structures of IrO_x, RuO_x, and $Ru_1Ir_1O_x$, and (c) Gibbes freedom of IrO_x, RuO_x, and $Ru_1Ir_1O_x$. Reproduced with permission from Ref. [154], © Wiley-VCH GmbH 2021. (d) Schematic illustration of HEA electrocatalysts with identified electronegativity-dependent preferences for active site adsorption of the intermediates OH* and H* during H_2O dissociation and H_2 production steps. (e) Raman spectrum of FeCoNiMnRu/CNFS in HER. (f) Comparison of PDOS of FeCoNiXRu (X = Mn, Cr, Cu) HEA. (g) FeCoNiMnRu HEA four stages of H_2O. Reproduced with permission from Ref. [157], © Hao, J. C. et al. 2022.

catalysts supported on CDs for enhanced HER performance. Liu et al. [164] synthesized Ru@SC-CDs using a hydrothermal method with garlic-derived CDs, achieving low overpotentials (59 mV in 0.5 M H_2SO_4, 66 mV in 1.0 M PBS, and 29 mV in 1.0 M KOH) (see Fig. 11(a) in Ref. [164]) and good cycling stability over 100 h. The excellent performance was attributed to the synergistic effect between SC-CDs and Ru nanoparticles.

Li et al. [165] prepared Ru@PC, Ru@CQDs, and Ru@P-AC using Porphyra as a precursor (see Fig. 11(b) from Ref. [165]). Among them, Ru@CQDs exhibited superior HER activity with a low Tafel slope (63 $mV \cdot dec^{-1}$) and overpotential (65 mV in 1.0 M KOH). The strong interaction between Ru nanoparticles and CQDs enhanced catalytic performance by preventing agglomeration.

Lu et al. [166] designed Ru1CoP/CDs, a composite of CoP nanoparticles doped with Ru single atoms on monolayer carbon nanosheets (see Fig. 11(c) from Ref. [166]). This catalyst exhibited extremely high HER efficiency with overpotentials of 51 and 49 mV under alkaline and acidic conditions, respectively. The doped Ru atoms lowered the energy barrier for proton coupling, enhancing catalytic performance.

These studies highlight the importance of structural design and synergistic interactions in optimizing the performance of Ru-based catalysts for HER applications.

The second category: the capture strategies. This approach involves introducing small molecules to immobilize metal active sites on an appropriate carbon matrix, thereby regulating the metallic active sites. For instance, multi-walled carbon nanotubes (MWCNTs) can be treated with acid to enrich their surfaces with carboxyl (–COOH) groups, which subsequently capture Ru nanoparticles (see Fig. 11(d) from Ref. [167]). Structural characterization has confirmed the presence of Ru nanoparticles and the formation of Ru–C and Ru–O bonds [167]. According to DFT calculations, the Ru–C bond is likely to serve as the primary active site of the catalyst. For example, adjusting the content of small molecules, as seen in NCPO-Ru NCS, can significantly influence and optimize the catalytic performance. This approach allows for fine-tuning the catalyst's activity and stability, making it more effective for various applications (see Fig. 11(e) from Ref. [168]). NCPO-Ru NCS can achieve catalysts with varying distributions and densities of Ru nano-clusters, which in turn influence the catalytic performance.

The third category: the nanoconfinement strategy. Ru nanoparticles is evenly confined on the carbon (Trinc) doped by C_3N_4 to enhance Ru HER activity (see Fig. 11(f) from Ref. [169]). The activity of Ru sites is optimized within the spatial restrictions of the carbon-based (MOF/COF). For example, Sun and others have prepared a high-active NiRu-BDC catalyst for HER by doping a single Ru atom to Ni-BDC, which consists of a layered structure constructed by coordinated octahedral divalent nickel and 1,4-benzenedicarboxylate (H_2BDC) (see Fig. 11(g) from Ref. [170]). The nickel hydroxide layers are directly coordinated and layered, while H_2BDC forms a three-dimensional framework. This unique structure of Ni-BDC provides a robust foundation for the subsequent incorporation of Ru single atoms. Single atoms Ru were introduced in Ni-BDC to adjust the electronic structure of Ni, thereby optimizing Ru adsorption capacity for H_2O and *H to improve the catalytic performance of catalysts. According to theoretical and experimental studies, the nanoconfinement strategy optimizes the charge transfer between Ru sites and carbon supports. The strategy can further weaken strong adsorption of *H on Ru sites.

Therefore, the optimal design strategy for Ru-based carbon composite materials involves creating porous structures and incorporating heteroatom doping. These approaches enable the

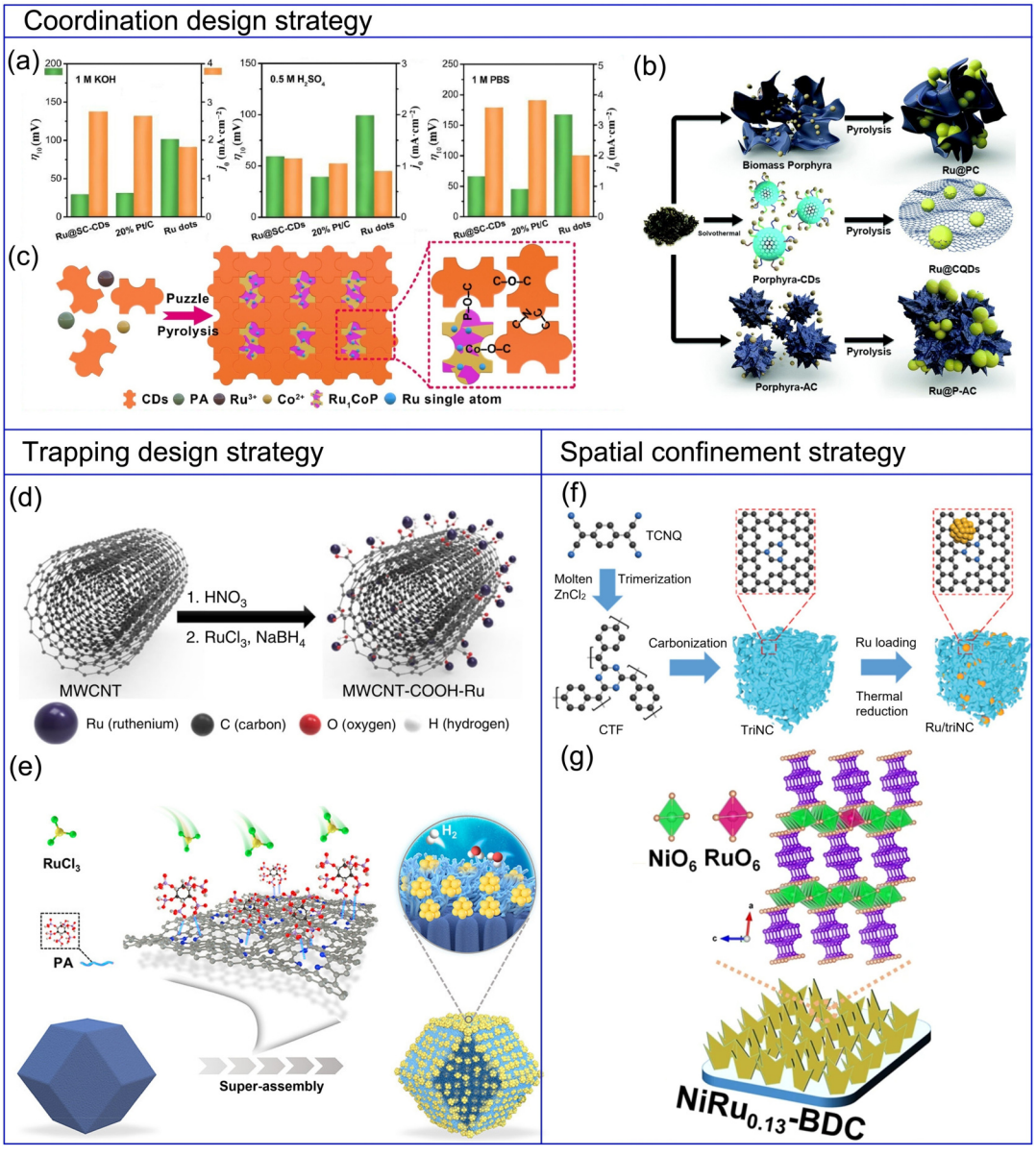

Figure 11 (a) Overpotential at a current density of 10 mA·cm^{-2} of Ru@SC-CDs in 1.0 M KOH, 0.5 M H_2SO_4, and 1.0 M PBS solutions. Reproduced with permission from Ref. [164], © Elsevier Ltd. 2019. All rights reserved. (b) Schematic illustration of the synthesis of the Ru@PC, Ru@CQDs, and Ru@P-AC. Reproduced with permission from Ref. [165], © The Royal Society of Chemistry and the Chinese Chemical Society 2020. (c) Synthesis and structure of Ru_1CoP/CDs @NSG. Reproduced with permission from Ref. [166], © Wiley-VCH GmbH 2021. (d) The synthetic roadmap of Ru@MWCNT catalyst. Reproduced with permission from Ref. [167], © Kweon, D. H. et al. 2020. (e) A schematic diagram of the Ru nano cluster by capturing-bond synthesis strategies. Reproduced with permission from Ref. [168], © American Chemical Society 2022. (f) Schematic diagram of the synthesis of Ru/trinc. Reproduced with permission from Ref. [169], © WILEY-VCH Verlag GmbH & Co. KGaA, Weinheim 2020. (g) Schematic diagram of $NiRu_{0.13}$-BDC catalyst. Reproduced with permission from Ref. [170], © Springer Nature 2021.

anchoring of various forms of Ru on the carbon matrix [171]. Additionally, by combining Ru with carbon materials, interactions such as electron transfer, spatial confinement, and defect effects can be leveraged. These strategies provide new insights for developing highly efficient and stable catalysts tailored for water splitting applications [172]. Despite these advancements, the development of Ru-based carbon composite catalysts still encounters several challenges: The interaction between Ru and carbon materials may alter the electronic structure of Ru, potentially reducing its activity in electrochemical applications, which remains an unresolved issue.

This review briefly introduces Ru-based catalysts from three perspectives: single-metal, dual-metal, and composite carbon materials. It is evident that researchers invested considerable effort into developing ruthenium [Ru]-based catalysts, aiming to achieve exceptional catalytic performance for water electrolysis. These endeavors highlight the growing focus on enhancing the efficiency and effectiveness of Ru-based materials in electrochemical applications. However, further improvements in Ru-based catalysts performance remain an area of ongoing research and exploration. Building on the existing catalysts, strategies to enhance their catalytic performance need continued investigation and development.

3.4 Strategies for enhancing Ru-based catalysts

From three perspectives—single-metal Ru, Ru alloys, and Ru-based carbon composite materials—the modification methods for Ru-

based catalysts are equally important. Understanding and mastering the reaction mechanisms of these catalysts is essential for optimizing their performance. By thoroughly investigating the catalytic processes, researchers can better modify Ru-based catalysts to enhance their efficiency and stability.

Presently, the optimization of Ru-based catalyst performance centers on various structural and compositional modifications, including atomic-level dispersion, alloying, size control, doping, defect engineering, and interface design. Irrespective of the specific method employed, the overarching goal is to improve catalytic efficiency by adjusting the electronic distribution at active sites and fine-tuning the dissolution and adsorption energies of reaction intermediates, based on the fundamental mechanisms of the HER and OER. These optimization strategies have garnered considerable acclaim within the scientific community and have significantly advanced the field. Nevertheless, achieving the ultimate objectives still presents considerable challenges. Continued research and innovation are necessary to bridge the gap between current achievements and the desired performance levels of Ru-based catalysts.

3.4.1 *Framework effects*

Modification strategies for Ru-based catalysts: framework effect. The control of catalyst size is a critical approach to enhancing catalytic activity. However, while smaller catalyst particles exhibit higher activity, they are prone to aggregation, leading to reduced atomic utilization and rapid deactivation. The framework effect involves the assembly of molecules or atoms into nanocomposite catalysts. By adjusting the nanoscale dimensions, the metal content can be minimized, thereby optimizing atomic utilization while preserving the catalyst's activity and stability [173]. The advantages of the framework effect are as follows: 1. Regulating the structure of metal nanocomposite catalysts stabilizes more active sites during catalytic reactions, resulting in higher atomic utilization and enhanced catalytic activity. 2. Incorporating metal active sites into the framework structure increases the number of active sites and modifies the electronic structure of the metal, thereby optimizing its catalytic performance. 3. The alteration of the electronic structure of the catalyst's metal sites through the framework effect optimizes the interaction between the metal active site and reaction intermediates, promoting more favorable catalytic pathways [174–177].

Different frameworks of catalysts, including 0D, 2D, and 3D structures, can be combined with 3D porous materials such as aerogels, metal foams, and hydrogels to form composite catalysts with distinct morphologies and catalytic properties (see Fig. 12 adapted from Ref. [174]). Subsequently, strategies such as doping, heterostructure, and core-shell architectures can be employed to further enhance the catalytic performance of these composite catalysts [178].

Ru nanoparticles catalysts typically exist in the form of 0D nanoparticles, 2D nanosheets, and complex 3D core-shell structures (Fig. 12). Among multi-dimensional materials, 3D porous materials such as aerogels, hydrogels, and metal foams are often utilized due to their excellent conductivity and abundant active sites, which facilitate the preparation of various Ru-based nanoparticle catalysts [179–182]. This approach enhances the catalytic performance of catalysts in water electrolysis environments. One prominent example of a 3D porous material is aerogel. Researchers have extensively used aerogels for catalyst preparation due to their high specific surface area, rich pore structure, and low density [183, 184]. The unique characteristics of aerogels provide numerous active sites, thereby enhancing the catalytic activity of aerogel-based catalysts [185, 186]. Aerogels are highly promising materials; some researchers have directly reduced metal precursors into metallic aerogels using sodium borohydride, resulting in excellent catalytic performance [187].

The framework effect, coupled with the utilization of advanced

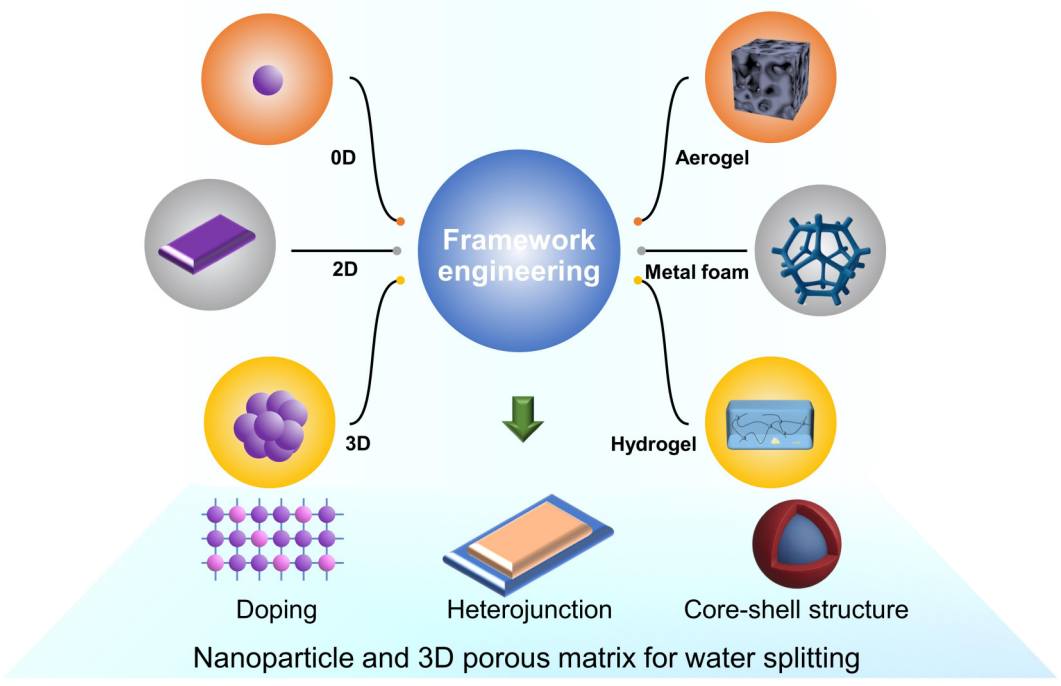

Figure 12 The particle catalysts of different forms (including 0D, 2D, and 3D) are used in framework engineering strategies and 3D porous matrix materials (gas gel, metal foam and hydrogel). Strategies such as doping, heterogeneity, and nuclear shell structure have improved the catalytic activity of catalyst. Adapted with permission from Ref. [174], @ Wiley-VCH GmbH 2024.

materials such as aerogels, hydrogels, and metal foams, presents substantial opportunities to significantly enhance the performance of ruthenium-based catalysts. By capitalizing on these strategies, researchers can engineer more efficient and stable catalysts for applications in water electrolysis and other catalytic processes. Future research endeavors should prioritize optimizing synthesis methodologies and investigating novel material combinations to fully exploit the advantages conferred by the framework effect.

3.4.2 *Doping regulation*

Doping regulation is also an effective method for modifying catalysts. Huang et al. [188] developed a solvothermal synthesis approach to create ultra-thin RuZn nanosheets (RuZn-NSS) with a unique structural configuration. This method allows for the precise formation of these nanosheets, which exhibit distinct morphological and structural characteristics. This material exhibits a Moiré superlattice structure and possesses abundant edge active sites. The results demonstrated that the RuZn-NSS catalyst exhibited excellent HER activity across a wide pH range. DFT calculations revealed that Zn anchoring on Ru-NSS lowers the d-band center of Ru sites, weakening the strong adsorption of the Ru-H bond (see Fig. 13(a) in Ref. [188]), thereby reducing water dissociation. This design provides valuable insights for developing efficient and low-cost Ru-based HER catalysts.

In addition to HER performance, another critical issue is OH_{ad} poisoning. Strong adsorption of OH_{ad} can lead to catalyst deactivation. Feng et al. [189] addressed this problem by combining Ru single atoms with SnO_2. During the reaction process, OH_{ad} primarily binds to SnO_2, which has a stronger affinity for OH_{ad} than Ru. This reduces the strong interaction between Ru and OH_{ad} during the HER process, allowing the Ru single atoms to remain active (see Fig. 13(b) from Ref. [189]). This effect significantly enhances the HER performance of the catalyst.

Furthermore, Sun et al. [190] prepared Ru-based catalysts with varying sizes, including single atoms, nano-clusters, and nanoparticles (see Fig. 13(c) from Ref. [190]). Among these, the Ru-NCS/NC catalyst exhibited the best catalytic performance. In 1.0 M KOH, 1.0 M phosphate buffer solution (PBS), and 0.5 M H_2SO_4, the overpotentials at a current density of 10 $mA{\cdot}cm^{-2}$ were 14, 30, and 32 mV, respectively. Stability tests showed that the catalyst maintained its performance for 50 h in 1.0 M KOH solution at a current density of 10 $mA{\cdot}cm^{-2}$. DFT calculations indicated that the strong interaction between Ru nano-clusters and N-doped carbon supports lowers the d-band center of Ru sites, reducing *H-adsorption on Ru sites and optimizing catalyst performance [191–194].

Doping and structural modifications have been demonstrated to be effective strategies for enhancing the performance of ruthenium-based catalysts in HER applications. By integrating ruthenium with other materials, optimizing electronic structures, and engineering heterogeneous interfaces, researchers can develop catalysts that exhibit high activity, stability, and cost-effectiveness. Future research should concentrate on further investigating the synergistic effects between different materials and refining synthesis methodologies to achieve superior catalytic performance.

3.4.3 *Defect effect*

Defect engineering holds significant potential for developing efficient and practical Ru-based catalysts. The defect structure in materials is closely related to the performance, activity, selectivity, and stability of catalysts, attracting increasing interest from researchers in defect design [195–197]. The electronic structure and surface/interface properties of precisely simulated Ru-based catalysts play a vital role. By introducing defects, one can carefully regulate adsorption energy [198–203]. Certain defects, such as stacking faults and dislocations, can enhance surface reactivity.

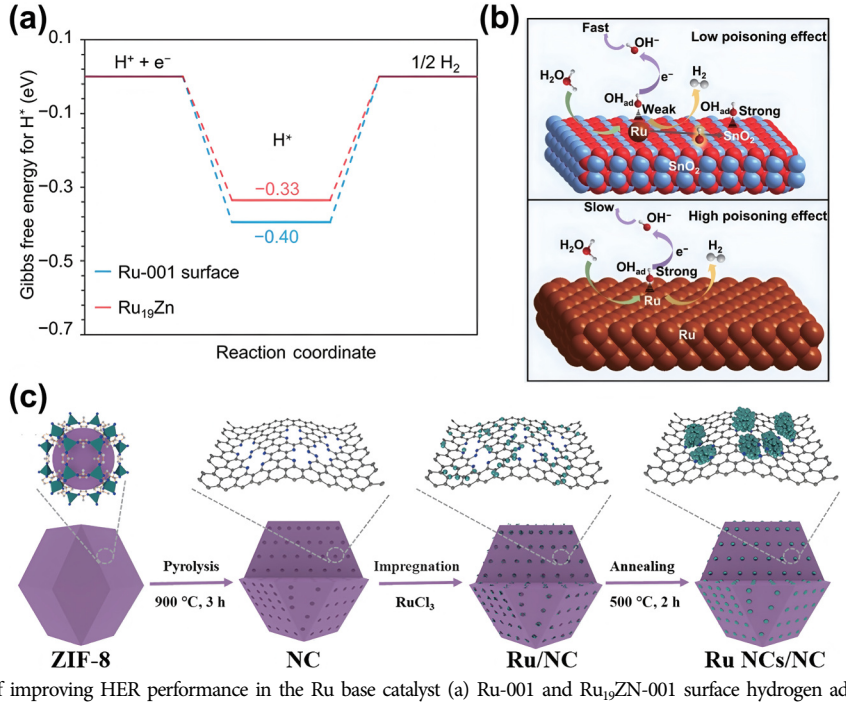

Figure 13 The mechanism of improving HER performance in the Ru base catalyst (a) Ru-001 and Ru_{19}ZN-001 surface hydrogen adsorption Gibbes freedom (*H) comparison. Reproduced with permission from Ref. [188], © Wiley-VCH GmbH 2023. (b) HER mechanism diagram of Ru-SnO_2/C. Reproduced with permission from Ref. [189], © Zhang, J. C. et al. 2022. Angewandte Chemie International Edition published by Wiley-VCH GmbH. (c) Ru NCS/NC synthesis flow chart. Reproduced with permissionfrom Ref. [190], © Tsinghua University Press 2023.

Niu et al. [204] proposed an effective strategy for the precise capture of single Ru atoms (Ru-SA/Pv-CoP_2) at the CoP_2 anion vacancy. Single Ru atoms could be well anchored to the anionic vacancies, thus establishing catalytic surfaces with the adjacent Co–P and Co–Ru coordination states and showing outstanding catalytic performance in the HER. This catalyst exhibited an unprecedented 17 mV overpotential at 10 mA·cm^{-2}. The prepared CoP_2 nanowires were annealed to produce an anionic P vacancy of CoP_2 (Pv-CoP_2). Ru ions in $RuCl_3$ solution were then electrostatically and thermally anchored to fill the P vacancies to obtain Ru-SA/Pv-CoP_2 (see Fig. 14(a) in Ref. [204]). The intro duction of Ru-SA into the P vacancy could effectively adjust the electronic behavior and coordinating environment of the Co sites in CoP_2. The introduction of Ru-SAs not only reversed the electronic state distribution (from the nucleophilic P-site to the electrophilic Ru-site), but also increased the number of states in the empty d-orbitals of Co, which increased the electrophilicity and accommodated more of the electrons transferred from the water, enabling efficient water adsorption and activation behavior. Jin and co-workers [205] used NiFe layered double hydroxides (LDHs) with different cation vacancies (M^{II} or M^{III}) as carriers to prepare a range of Ru SACs with variable geometrical and electronic structures. The synthesis process is shown in Fig. 14(b). Among various (hydroxide) oxides, layered double hydroxides (LDHs) were generally formulated as $M^{II}_{1-x}M^{III}_x(OH)_2(A^{n-}_{x/n})\cdot mH_2O$ (where M^{II} is a divalent metal, M^{III} is a trivalent metal, and A^{n-} is the interlayer anion), which had rich alkaline active sites and adjustable components. M^{III} or M^{II} cation vacancies could be formed in LDHs [206]. Because of the net trap confinement effect, these cations were isolated by atoms in the LDH framework, which served to stabilize the metal single atoms, resulting in SACs of various well-defined microenvironments. The stability of Ru_1/LDH-V^{III} in the benzyl alcohol oxidation reaction was enhanced by the larger oxidation state and fewer filled d-state electrons of Ru1 and a more intense metal–carrier interaction. DFT calculations further showed that the unique coordination environment of Ru1 enhanced the desorption of benzaldehyde and improved the catalytic activity of Ru_1/LDH-V^{III} for benzyl alcohol oxidation.

In addition to metal vacancies, heteroatom vacancies are often used to modify catalysts, such as S vacancies, O vacancies, and P vacancies. Zhou group [207] fabricated a composite catalyst consisting of Ru NPs supported on mesoporous TiO_2. When operated at a current density of 10 mA·cm^{-2}, the catalyst exhibited an overpotential of 15 mV. Additionally, it achieved a turnover frequency (TOF) of 8.74 s^{-1} at an overpotential of 100 mV, highlighting its efficient catalytic performance under these conditions. DFT results revealed the reaction mechanism: during the HER process, water activation occurs on the support (R-TiO_2), and oxygen vacancies promote the desorption of *OH, preventing *OH poisoning. These studies provide a foundation for constructing Ru-based catalysts with enhanced defective effects. Finally, we summarize the Ru catalysts, synthesis methods and catalytic reactions to facilitate better understanding and application of ruthenium-based catalysts (Table 1).

3.5 Stability of ruthenium-based catalysts and applications in industry

3.5.1 *Applications in HER*

Lu et al. [208] reported a hybrid material, Ru-M (M = Ni, Mn, Cu) bimetallic nanoparticles and carbon quantum dots (RuM/CQDs), for the efficient HER. During synthesis, the abundant functional groups (–COOH and –OH) on the surfaces of the CQDs can coordinate with the RuM ions with empty d orbitals to form a relatively stable CQDs-Ru ion coordination composite. The RuM NPs are restricted between the CQDs to form ultrafine nanocrystals with stable structures that effectively prevent the agglomeration and growth of the NPs during the reaction [209]. The catalyst has excellent HER performance at different pH. In particular, the RuNi/CQDs show small overpotential at 10 mA·cm^{-2} (13 mV at 1 M KOH, 58 mV at 0.5 M H_2SO_4, and 18 mV at 1 M PBS) and long-term durability in acidic, neutral, and alkaline media after 10,000 cycles.

Baek et al. [210] reported that highly dispersed Ru particles (2 nm) loaded on graphene (Ru@GnP) exhibited excellent HER activity in acidic and alkaline media. The synthesis of Ru@GnP was carried out in two steps: synthesis of the support and reduction of the metal loading. Graphene nanosheets (CGnP) functionalized with edge carboxylic acids were prepared by ball milling of graphite in the presence of dry ice. Subsequently, Ru ions were bound to CGnP, and Ru@GnP was synthesized after reduction and annealing treatments. In this process, the abundant carboxylic acid groups on the support coordinated with the Ru ions and enhanced the binding of Ru ions to the support, thus increasing the loading of Ru. The prepared Ru@GnP showed smaller overpotentials (13 mV in 0.5 M H_2SO_4 and 22 mV in 1 M KOH) and lower Tafel slopes (30 mV·dec^{-1} in 0.5 M H_2SO_4 and 28 mV·dec^{-1} in 1 M KOH) at 10 mA·cm^{-2}. In addition, after 10,000 long-term durability tests, the carrier maintained a highly dispersed morphology as its high surface area (403.04 m^2·g^{-1}) prevented Ru particles from aggregating in the reaction. The excellent stability of ruthenium-based catalysts is due to the presence of the support, which is therefore essential for the stability of ruthenium-based catalysts.

3.5.2 *Applications in OER*

Generally speaking, with a high catalyst loading up to 1–2 mg·cm^{-2}, the membrane electrodes were operated at around 500 mA·cm^{-2} in alkaline water electrolysis while beyond 1.6 A·cm^{-2} in proton exchange membrane water electrolysis [211]. However, in voluminous cases, the powder-type catalysts generally are mixed with the additional binder and carbon conductor to integrate onto the current collector, leading to increased resistance, covered active sites, unfavorable mass transportation, limited catalyst loading (< 1 mg·cm^2), and the oxidation of conductive carbon. The generated large number of bubbles causes the catalysts to fall off easily from the assembled electrode under large current density. Thus, the freestanding electrodes emerge as the practical application requirement of achieving a large current density of 400–1600 mA·cm^{-2} when the cell voltage is between 1.8–2.4 V. For example, the self-supporting Ru single atom anchored on FeCo-LDH(Ru_xSACs@FeCo-LDH) shows the low OER overpotentials of 194 and 246 mV at corresponding 10 and 1000 mA·cm^{-2}, respectively, and survives at 1000 mA·cm^{-2} for more than 1000 h [212]. The freestanding NiMo-NH_3/H_2 catalyst presents an attractive HER activity and delivers only overpotentials of 11 and 107 mV at current densities of 10 and 500 mA·cm^{-2}, respectively, while Fe-doped NiMo–NH_3/H_2 catalyst only requires OER overpotentials of 244 mV at 500 mA·cm^{-2} [213]. When NiMo-NH_3/H_2 and Fe-doped NiMo-NH_3/H_2 were integrated into an AEM electrolyze and tried at 80 °C in 1 M KOH, it took only 1.57 V to reach 1000 mA·cm^2.

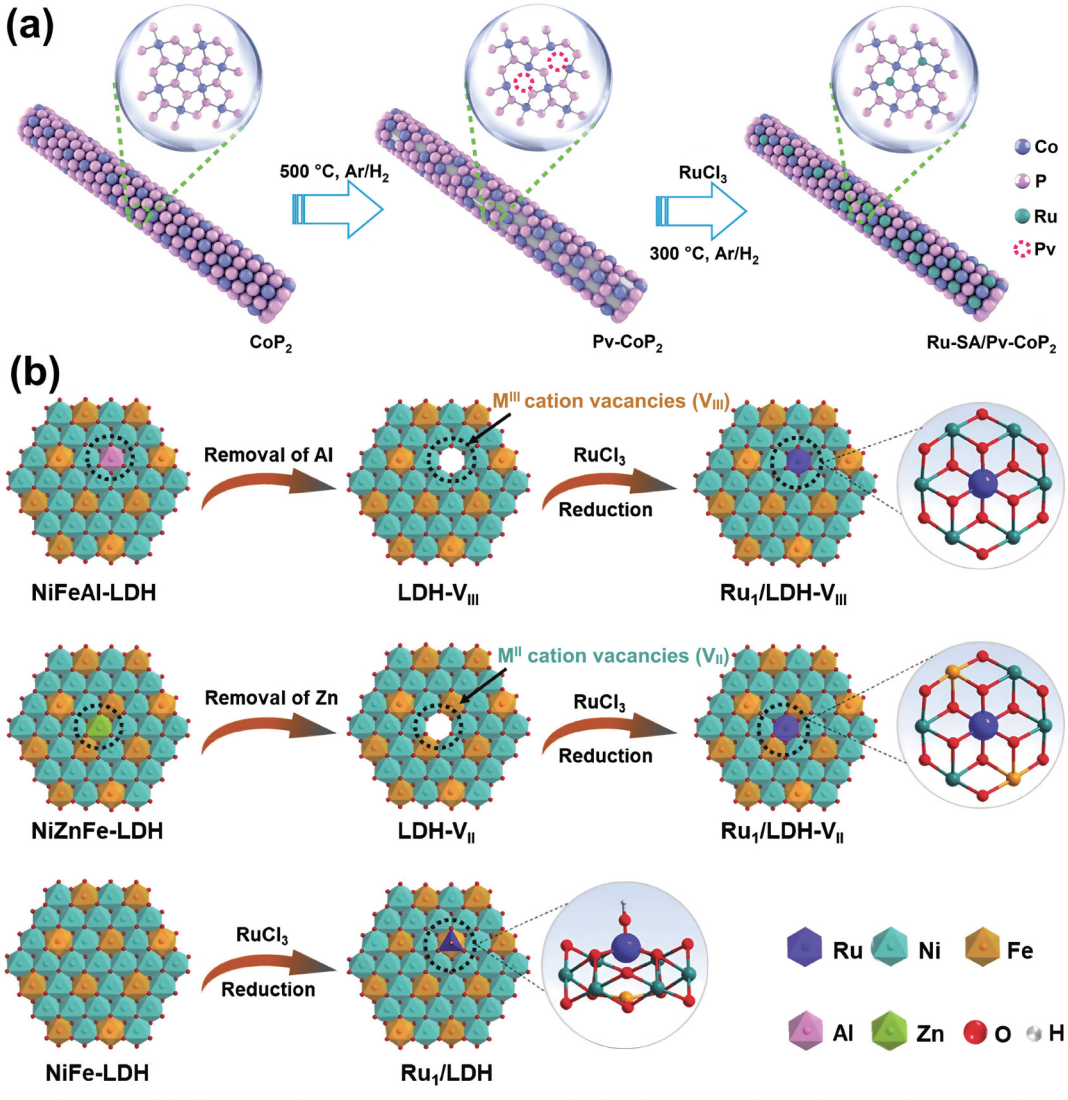

Figure 14 Schematic illustration of the fabrication of (a) Ru-SA/Pv-CoP_2 NWs. Reproduced with permission from Ref. [204], Wiley-VCH GmbH 2022. (b) Ru1/LDH-VIII, Ru1/LDH-VII, and Ru1/LDH by defect engineering strategy. Reproduced with permission from Ref. [205], Wiley-VCH GmbH 2021.

Table 1 Summary of Ru-based catalysts, synthesis methods, and applications

Catalyst type	Synthesis method	Application	Reference
Single-metal Ru-based catalysts	Adjusting atomic arrangement to design crystal phases	HER, OER	[126–140]
Ru single-atom catalysts	Supported on nitrogen-doped carbon via hydrothermal or solvothermal methods	HER, OER	[141, 142]
Ru-based alloy catalysts	Alloying with other metals (e.g., Rh, Ir, Pt, Fe, Co, Ni, Cu, Cr, Mn)	HER, OER	[143–159]
Ru-coupled carbonnanocatalysts	Hydrothermal synthesis, solvothermal synthesis, nanoconfinement strategies	HER, OER	[160–172]
Ru nanoparticles (0D, 2D, 3D)	Framework engineering, doping, heterostructure, core-shell architectures	HER, OER	[178–186]
Ru-based defect-engineeredcatalysts	Vacancy engineering (e.g., Co vacancies, P vacancies, S vacancies, O vacancies)	HER, OER	[204–207]

Hou's group reported a hierarchical bimetal $NiMoO_x/NiMoS_x$ heterostructure arrays consisting of 2D MoO_x/MoS_2 nanosheets and 1D NiO_x/Ni_3S_2 nanorods. It not only showed attractive small overpotentials of 38 and 186 mV at 10 mA·cm^{-2} for HER and OER, respectively, but also exhibited the promisingly low cell voltages of 1.60 and 1.66 V for overall water splitting under corresponding 0.5 and 1 A·cm^{-2}, respectively [177]. The unique structure of multi-interface bimetal $NiMoO_x/NiMoS_x$ arrays not only afforded fast mass transformation and bubble detachment but also improved conductivity and provided sufficient active sites. Conspicuously, the self-supported electrode possesses advantages beyond comparison, firstly, it could omit the complicated post-coasting process and thus simplify the electrode preparation procedure; secondly, the in situ growth of the catalyst on the substrate ensures the compact contact to facilitate the electron transmission and avoid the catalysts shedding; thirdly, the three-dimensional open structure of substrate could undoubtedly favor the mass transport and increase the catalyst loading for providing sufficient active sites [214]; fourthly, the sophisticated morphology and structure modifications help to tune the hydrophilicity and hydrophobicity for expediting the

bubble detachment and benefiting the re-contact between active sites and electrolyte.

3.6 Precious metal catalysts for seawater electrolysis

With the increasing utilization of hydrogen energy, electrolytic hydrogen production technology has also advanced. However, freshwater resources on Earth are limited and far less abundant than seawater. Compared to freshwater electrolysis, seawater electrolysis holds greater potential for future energy development. Seawater electrolysis can emulate the process of water electrolysis by applying similar technologies to seawater (see Fig. 15 from Ref. [56]). However, the presence of abundant cations such as calcium and magnesium ions in seawater leads to their deposition on the cathode surface during electrolysis [215]. Long-term deposition increases the pH value at the cathode surface, promoting sediment accumulation and hindering gas release [216–220]. Due to the complex environment and composition of seawater [including microorganisms, organic and inorganic impurities], the challenges are more severe. Additionally, the presence of chloride ions (Cl^-) in seawater can lead to side reactions, such as the chlorine oxidation reaction [ClOR] on the anode, which not only affects catalyst performance but also produces toxic chlorine byproducts [111, 221].

Seawater electrolysis also presents several challenges. Changes in pH near the electrode surface can lead to catalyst degradation and magnesium hydroxide precipitation due to increased local pH at the cathode [222, 223], thereby hindering further catalytic reactions (see Fig. 16(a) from Ref. [224]). To stabilize the pH during seawater electrolysis, it is essential to replenish the electrolyte promptly.

In addition, other ions and microorganisms in seawater can also poison the catalyst, thereby reducing its stability. To address these challenges, researchers have developed high-selectivity membranes that serve as barriers to filter impurities and protect the cathode (Fig. 16(b) from Ref. [224]). Furthermore, a selective permeation layer is applied to the catalyst surface to maintain normal catalytic performance (Fig. 16(c) from Ref. [224]). Simultaneously, designing high-selective catalysts plays a crucial role in preventing the formation of toxic chlorine gas during seawater electrolysis. Recent advancements have enabled seawater electrolytic cells to operate successfully under both neutral and alkaline conditions. This progress highlights the critical need to identify catalysts that not only demonstrate high activity but also maintain stability in these environments. Ensuring these properties is vital for the safe and efficient operation of seawater electrolysis systems [225–230].

For instance, the research team headed by Gao employed formic acid as a reducing agent and graphdiyne as a support material to synthesize Rh nanocrystals [Rh/GDY] in an aqueous environment (see Fig. 16(d) from Ref. [231]). The SP–C–Rh bond in the catalyst serves a dual purpose: it stabilizes the Rh nanocrystals and significantly enhances their charge transfer capacity. Experimental data reveal that Rh/GDY achieves a remarkable current density of 1000 $mA{\cdot}cm^{-2}$ with an overpotential of just 65 mV, surpassing the performance of other reported catalysts and 20 wt.% Pt/C in a 1.0 M KOH + 0.5 M NaCl solution. The Tafel slope for this catalyst is measured at 21 $mV{\cdot}dec^{-1}$ (see Figs. 16(e) and 16(f) from Ref. [231]), indicating efficient reaction kinetics. Notably, after 8,000 cyclic voltammetry (CV) cycles, the overpotential of Rh/GDY remains unchanged (see Fig. 16(g) from Ref. [231]), highlighting its exceptional stability. Figures 16(h) and 16(i) show that although the proportions of Rh^0, Rh^+, and Rh^{3+} fluctuate during the cycling test, the overall catalytic activity of Rh/GDY remains stable. These observations underscore the importance of mixed-valence states in achieving high catalytic performance, rather than relying on a single-valence state.

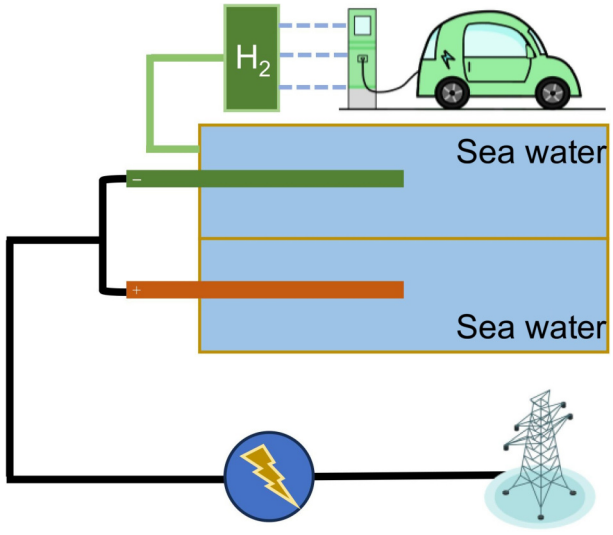

Figure 15 Illustrative diagrams on industrial electrocatalytic seawater decomposition. Adapted with permission from Ref. [56]. © Wiley-VCH GmbH 2023.

In recent years, a high-performance and corrosion-resistant RuMoNi catalyst for electrolytic seawater has been developed through hydrothermal and electrochemical activation methods [131]. This catalyst features an array of surface porous nanorods. High-resolution transmission electron microscopy (HRTEM) revealed that the catalyst comprises a Ni_4Mo alloy conductive substrate, a RuO_2/NiOOH active phase, and a $NiMoO_4$ corrosion-resistant layer. In an electrolyte consisting of 1 M KOH and seawater, the RuMoNi electrocatalyst exhibits an OER overpotential of merely 245 mV at a current density of 100 $mA{\cdot}cm^{-2}$ and achieves a high current density of 1000 $mA{\cdot}cm^{-2}$ at 1.7 V vs. RHE. The RuMoNi electrocatalyst demonstrates excellent stability and activity in alkaline solutions, including lye, alkaline salt solutions, and alkaline seawater electrolytes, with nearly 100% OER selectivity in seawater electrolytes.

The construction of unique (Co) Lewis acid and (Ru–P) base pairs in Ru-Co_2P decorated on nitrogen-phosphorus co-doped carbon (Ru-Co_2P/NPC) significantly optimizes the energy barrier for hydrolytic dissociation and enhances the corrosion resistance during alkaline seawater decomposition. As anticipated, the optimal Ru-Co_2P/NPC-2 exhibited superior HER performance, achieving overpotentials as low as 22.0 and 26.0 mV at 10 $mA{\cdot}cm^{-2}$ in alkaline and alkaline seawater electrolytes [232], respectively. Furthermore, it demonstrated stable operation at 50 $mA{\cdot}cm^{-2}$ for over 30 h. Experimental and theoretical results indicate that Co, acting as a Lewis acid site, facilitates water adsorption and H–O bond cleavage, while Ru–P, functioning as a Lewis base site, promotes hydrogen desorption in alkaline media. Additionally, the modulated chemical microenvironment effectively mitigates chloride-induced corrosion at the catalyst's active sites.

3.7 Industrial-scale challenges and opportunities of Ru-based catalysts in seawater electrolysis

The industrial application of Ru-based catalysts in seawater

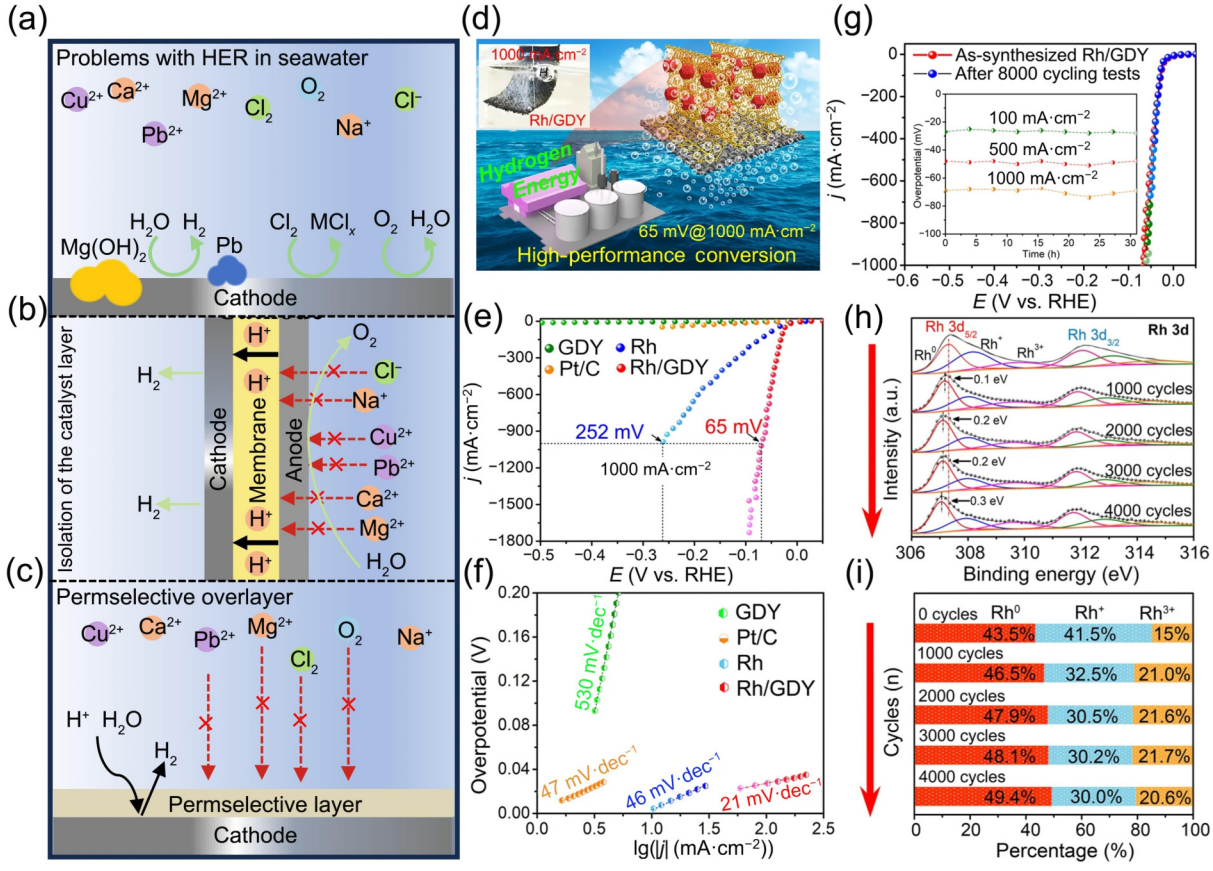

Figure 16 (a) Schematic diagram of impurities deposition and catalyst corrosion. (b) The design schematic of the appropriate membrane to prevent catalysts from being inactivated. (c) Schematic diagram of the selected cover layer of the unwavering material on the surface of the catalyst. Reproduced with permission from Ref. [224], © Springer Nature 2020. (d) Efficient hydrogen evolution on Rh/GDY, (e) polarization curve, (f) Tagar's slope, (g) Rh/GDY is durable at 100, 500 and 1000 mA·cm^{-2} test, (h) Rh/GDY's Rh XPS spectra obtained after stability testing, (i) species atom percentage in the durability experiment. Reproduced with permission from Ref. [231], © Gao, Y. et. al. 2022.

electrolysis presents both significant challenges and promising opportunities. While Ru-based catalysts have demonstrated exceptional catalytic performance in laboratory settings, their large-scale implementation requires addressing several critical factors, including cost, long-term stability, and scalability.

3.7.1 Cost

Ru-based catalysts, although more cost-effective than Pt-based materials, still face economic constraints when scaled up for industrial use. The high initial cost of Ru and the need for sophisticated synthesis techniques can limit their widespread adoption. Recent studies have focused on reducing Ru loading while maintaining or enhancing catalytic performance. For example, the development of single-atom Ru catalysts and Ru-based HEAs has shown potential for cost reduction without compromising activity [233].

3.7.2 Long-term stability

The long-term stability of Ru-based catalysts in the harsh environment of seawater electrolysis is a major concern. Seawater contains various ions and impurities that can lead to catalyst degradation over time. Strategies such as doping with stabilizing elements and designing protective layers have been explored to enhance the durability of Ru catalysts. For instance, the incorporation of oxygen vacancies in RuO_2 has been shown to improve its stability in acidic and alkaline media [234].

3.7.3 Scalability

Scaling up Ru-based catalysts for industrial applications requires not only maintaining their catalytic performance but also ensuring reproducibility and consistency in large batches. Recent advancements in the synthesis of Ru-based catalysts using scalable methods, such as hydrothermal synthesis and electrochemical activation, have shown promise in addressing this challenge. For example, the development of RuMoNi catalysts through hydrothermal methods has demonstrated excellent performance and stability in alkaline seawater electrolytes [131].

In summary, while Ru-based catalysts offer significant potential for efficient seawater electrolysis, their industrial-scale application requires continued research and development to address cost, stability, and scalability issues. Future work should focus on optimizing synthesis methods, reducing material costs, and enhancing catalyst durability to make Ru-based catalysts a viable option for large-scale hydrogen production from seawater.

4 Conclusions and outlook

Ru-based catalysts are considered the ideal candidates for electrolytic water catalysis due to their cost-effectiveness and exceptional catalytic performance. Current efforts to enhance the performance of Ru-based catalysts predominantly focus on various structural and compositional modifications, including atomic

dispersion, alloying, dimensional effects, controlled doping, and defect engineering. Irrespective of the specific strategy employed, these optimization techniques consistently revolve around the fundamental mechanisms of HER and OER. The primary goals of these optimizations are to adjust the electronic distribution at active sites and optimize the adsorption and desorption energies of reaction intermediates. By doing so, researchers aim to improve catalytic efficiency and stability. Despite significant progress, several challenges remain in fully realizing the potential of Ru-based catalysts for water electrolysis. Continued research is necessary to address these challenges and develop more effective catalysts that can meet the demands of large-scale applications.

(1) Understanding the relationship and designing excellent catalysts based on this insight requires researchers to continuously strive to gather information through data analysis and in situ characterization techniques. Data sources include both experimental and computational data. For instance, Raman spectroscopy, SEM, XRD, and XPS can provide insights into the combined interactions and electronic structure of catalysts. By analyzing these data, researchers can better understand the reaction mechanisms of catalysts, thereby contributing to their development and optimization.

(2) Although many Ru-based catalysts exhibit the stability in alkaline or acidic environments, their stability and the influencing factors under harsh conditions require further exploration at the atomic and molecular levels during electrocatalytic water splitting.

(3) The primary technical barrier in seawater electrolysis is the competitive reaction between the OER and the ClOR, which significantly affects the selectivity of oxygen on Ru-based catalysts, thereby impacting the overall catalytic activity and efficiency in seawater electrolytes. Therefore, designing catalysts with low OER overpotential and abundant active sites, along with an appropriate protective layer, is a critical research direction for improving seawater electrolyte catalysts.

(4) By developing a range of novel theoretical calculation models, a unique catalyst model was established to investigate how to enhance the synergy between low mass transfer efficiency and electron transfer effects in Ru-based catalysts. This approach aims to analyze and elucidate the structure-activity relationship of Ru-based catalysts in water electrolysis.

(5) The electronic structure and atomic utilization of Ru-based catalysts during water electrolysis were significantly enhanced through precise modification of the microenvironment surrounding the Ru sites.

(6) Based on the Ru sites, multi-metal sites were designed and integrated with non-metal active sites to construct a novel multi-point collaborative catalytic system for water electrolysis. This approach aims to achieve efficient and stable hydrogen evolution during electrolytic water splitting at ampere-level current densities.

Data availability

All data needed to support the conclusions in the paper are presented in the manuscript. Additional data related to this paper may be requested from the corresponding author upon request.

Acknowledgements

This work was supported by the National Natural Science Foundation of China (No. 22279118), the National Science Fund for Distinguished Young of China (No. 22225202), the Special Projects of Henan Province Key Research and Development and Promotion (Science and Technology Research) (No. 232102241033), and the Young Top Talent Program of Zhongyuan-Yingcai-Jihua (No. 30602674).

Declaration of competing interest

All the contributing authors report no conflict of interests in this work.

Author contribution statement

K. Z.: Investigation, literature review, formal analysis, writing – original draft, writing – review & editing, graphic arrangement. K. W.: Literature review, graphic arrangement, format arrangement. S. M. C.: Document search, format check, graphic arrangement. L. Y. W.: Literature search, grammar modification. H. Y. L.: Literature review, text polishing. Y. Y. L.: format analysis, writing – original draft, software. Y. F. W. Grammar checks, format analysis, and paper polishing. J. C. J.: Format review/analysis. B. J. L.: Supervised, conceived, writing – review & editing, and designed the project.

Use of AI statement

None.

References

[1] Chien, F.; Chau, K. Y.; Ady, S. U.; Zhang, Y. Q.; Tran, Q. H.; Aldeehani, T. M. Does the combining effects of energy and consideration of financial development lead to environmental burden: Social perspective of energy finance. *Environ. Sci. Pollut. Res.* **2021**, *28*, 40957–40970.

[2] Njoh, A. J. A Systematic review of environmental determinants of renewable energy performance in Ethiopia: A PESTECH analysis. *Renew. Sustain. Energy Rev.* **2021**, *147*, 111243.

[3] Welch, J. B.; Venkateswaran, A. The dual sustainability of wind energy. *Renew. Sustain. Energy Rev.* **2009**, *13*, 1121–1126.

[4] Martínez Ceseña, E. A.; Mancarella, P. Energy systems integration in smart districts: Robust optimisation of multi-energy flows in integrated electricity, heat and gas networks. *IEEE Trans. Smart Grid* **2019**, *10*, 1122–1131.

[5] Lund, H.; Østergaard, P. A.; Chang, M.; Werner, S.; Svendsen, S.; Sorknæs, P.; Thorsen, J. E.; Hvelplund, F.; Mortensen, B. O. G.; Mathiesen, B. V. et al. The status of 4th generation district heating: Research and results. *Energy* **2018**, *164*, 147–159.

[6] Mathiesen, B. V.; Lund, H.; Connolly, D.; Wenzel, H.; Østergaard, P. A.; Möller, B.; Nielsen, S.; Ridjan, I.; Karnøe, P.; Sperling, K. et al. Smart energy systems for coherent 100% renewable energy and transport solutions. *Appl. Energy* **2015**, *145*, 139–154.

[7] Hoang, A. T.; Pham, V. V.; Nguyen, X. P. Integrating renewable sources into energy system for smart city as a sagacious strategy towards clean and sustainable process. *J. Cleaner Prod.* **2021**, *305*, 127161.

[8] Connolly, D.; Lund, H.; Mathiesen, B. V. Smart Energy Europe: The technical and economic impact of one potential 100% renewable energy scenario for the European union. *Renew. Sustain. Energy Rev.* **2016**, *60*, 1634–1653.

[9] Yang, R.; Zheng, X. Z.; Qin, M. K.; Lin, B. B.; Shi, X. Y.; Wang, Y. A trifunctional Ni–P/Fe–P collaborated electrocatalyst enables self-powered energy systems. *Adv. Sci.* **2022**, *9*, 2201594.

[10] Tang, C.; Zhang, R.; Lu, W. B.; Wang, Z.; Liu, D. N.; Hao, S.; Du, G.; Asiri, A. M.; Sun, X. P. Energy-saving electrolytic hydrogen generation: Ni_2P nanoarray as a high-performance non-noble-metal electrocatalyst. *Angew. Chem., Int. Ed.* **2017**, *56*, 842–846.

[11] Zhao, X.; Li, W. P.; Cao, Y. H.; Portniagin, A.; Tang, B.; Wang, S. X.; Liu, Q.; Yu, D. Y. W.; Zhong, X. Y.; Zheng, X. R. et al. Dual-atom Co/Ni electrocatalyst anchored at the surface-modified $Ti_3C_2T_x$ MXene enables efficient hydrogen and oxygen evolution reactions. *ACS Nano* **2024**, *18*, 4256–4268.

[12] Zhou, Q. W.; Shen, Z. H.; Zhu, C.; Li, J. C.; Ding, Z. Y.; Wang, P.; Pan, F.; Zhang, Z. Y.; Ma, H. X.; Wang, S. Y. et al. Nitrogen-doped CoP electrocatalysts for coupled hydrogen evolution and sulfur generation with low energy consumption. *Adv. Mater.* **2018**, *30*, 1800140.

[13] Hanan, A.; Lakhan, M. N.; Shu, D.; Hussain, A.; Ahmed, M.; Soomro, I. A.; Kumar, V.; Cao, D. X. An efficient and durable bifunctional electrocatalyst based on PdO and Co_2FeO_4 for HER and OER. *Int. J. Hydrogen Energy* **2023**, *48*, 19494–19508.

[14] Huang, B.; Xu, H. Y.; Jiang, N. N.; Wang, M. H.; Huang, J. R.; Guan, L. H. Tensile-strained RuO_2 loaded on antimony-tin oxide by fast quenching for proton-exchange membrane water electrolyzer. *Adv. Sci.* **2022**, *9*, 2201654.

[15] Wu, Z. Y.; Chen, F. Y.; Li, B. Y.; Yu, S. W.; Finfrock, Y. Z.; Meira, D. M.; Yan, Q. Q.; Zhu, P.; Chen, M. X.; Song, T. W. et al. Non-iridium-based electrocatalyst for durable acidic oxygen evolution reaction in proton exchange membrane water electrolysis. *Nat. Mater.* **2023**, *22*, 100–108.

[16] Chen, D.; Yu, R. H.; Yu, K. S.; Lu, R. H.; Zhao, H. Y.; Jiao, J. X.; Yao, Y. T.; Zhu, J. W.; Wu, J. S.; Mu, S. C. Bicontinuous RuO_2 nanoreactors for acidic water oxidation. *Nat. Commun.* **2024**, *15*, 3928.

[17] Wu, Y.; Yao, R.; Zhao, Q.; Li, J. P.; Liu, G. La-RuO_2 nanocrystals with efficient electrocatalytic activity for overall water splitting in acidic media: Synergistic effect of La doping and oxygen vacancy. *Chem. Eng. J.* **2022**, *439*, 135699.

[18] Rong, C. L.; Shen, X. J.; Wang, Y.; Thomsen, L.; Zhao, T. W.; Li, Y. B.; Lu, X. Y.; Amal, R.; Zhao, C. Electronic structure engineering of single-atom Ru sites via Co–N_4 sites for bifunctional pH-universal water splitting. *Adv. Mater.* **2022**, *34*, 2110103.

[19] Hu, C.; Yue, K. H.; Han, J. J.; Liu, X. Z.; Liu, L. J.; Liu, Q. N.; Kong, Q. Y.; Pao, C. W.; Hu, Z. W.; Suenaga, K. et al. Misoriented high-entropy iridium ruthenium oxide for acidic water splitting. *Sci. Adv.* **2023**, *9*, eadf9144.

[20] Jia, Z. M.; Qin, X. T.; Chen, Y. L.; Cai, X. B.; Gao, Z. R.; Peng, M.; Huang, F.; Xiao, D. Q.; Wen, X. D.; Wang, N. et al. Fully-exposed Pt–Fe cluster for efficient preferential oxidation of CO towards hydrogen purification. *Nat. Commun.* **2022**, *13*, 6789.

[21] Ishaq, H.; Dincer, I.; Crawford, C. A review on hydrogen production and utilization: Challenges and opportunities. *Int. J. Hydrogen Energy* **2022**, *47*, 26238–26264.

[22] Zhao, K. Y.; Jia, C. Q.; Li, Z. H.; Du, X. Z.; Wang, Y. B.; Li, J. J.; Yao, Z. C.; Yao, J. Recent advances and future perspectives in carbon capture, transportation, utilization, and storage (CCTUS) technologies: A comprehensive review. *Fuel* **2023**, *351*, 128913.

[23] Geels, F. W.; Kern, F.; Fuchs, G.; Hinderer, N.; Kungl, G.; Mylan, J.; Neukirch, M.; Wassermann, S. The enactment of socio-technical transition pathways: A reformulated typology and a comparative multi-level analysis of the German and UK low-carbon electricity transitions (1990–2014). *Res. Policy* **2016**, *45*, 896–913.

[24] Martin, C. J. The sharing economy: A pathway to sustainability or a nightmarish form of neoliberal capitalism. *Ecol. Econ.* **2016**, *121*, 149–159.

[25] Lindberg, M. B.; Markard, J.; Andersen, A. D. Policies, Actors and sustainability transition pathways: A study of the EU's energy policy mix. *Res. Policy* **2019**, *48*, 103668.

[26] Martin, G.; Pujos, L.; Magrini, M. B. Micro-level sustainability transition pathways of institutional food services in France. *Front. Sustain. Food Syst.* **2022**, *6*, 943020.

[27] Lin, R.; Hu, Q.; Liu, Z. L.; Pan, S. S.; Chen, Z. F.; Zhang, W.; Liu, Z. Y.; Zhang, S. L.; Zhang, C. Y. Integrated CuO/Pd nanospike hydrogen sensor on silicon substrate. *Nanomaterials* **2022**, *12*, 1533.

[28] Osman, A. I.; Mehta, N.; Elgarahy, A. M.; Hefny, M.; Al-Hinai, A.; Al-Muhtaseb, A. H.; Rooney, D. W. Hydrogen production, storage, utilisation and environmental impacts: A review. *Environ. Chem. Lett.* **2022**, *20*, 153–188.

[29] Peng, X.; Xie, S.; Wang, X.; Pi, C. R.; Liu, Z. T.; Gao, B.; Hu, L. S.; Xiao, W.; Chu, P. K. Energy-saving hydrogen production by the methanol oxidation reaction coupled with the hydrogen evolution reaction Co-catalyzed by a phase separation induced heterostructure. *J. Mater. Chem. A* **2022**, *10*, 20761–20769.

[30] Özhava, D.; Özkar, S. Nanoalumina-supported rhodium(0) nanoparticles as catalyst in hydrogen generation from the methanolysis of ammonia borane. *Mol. Catal.* **2017**, *439*, 50–59.

[31] Pu, Z. H.; Zhao, J. H.; Amiinu, I. S.; Li, W. Q.; Wang, M.; He, D. P.; Mu, S. C. A universal synthesis strategy for P-rich noble metal diphosphide-based electrocatalysts for the hydrogen evolution reaction. *Energy Environ. Sci.* **2019**, *12*, 952–957.

[32] Sun, H. C.; Li, L. F.; Humayun, M.; Zhang, H. M.; Bo, Y. N.; Ao, X.; Xu, X. F.; Chen, K.; Ostrikov, K.; Huo, K. F. et al. Achieving highly efficient pH-universal hydrogen evolution by superhydrophilic amorphous/crystalline $Rh(OH)_3$/NiTe coaxial nanorod array electrode. *Appl. Catal. B: Environ.* **2022**, *305*, 121088.

[33] Akbayrak, S.; Özkar, S. Ammonia norane as hydrogen storage materials. *Int. J. Hydrogen Energy* **2018**, *43*, 18592–18606.

[34] Lee, J.; Ga, S.; Lim, D.; Lee, S.; Cho, H.; Kim, J. Carbon-free green hydrogen production process with induction heating-based ammonia decomposition reactor. *Chem. Eng. J.* **2023**, *457*, 141203.

[35] Yun, S.; Im, J.; Kim, J.; Cho, H.; Lee, J. Enhanced ammonia-cracking process via induction heating for green hydrogen: A comprehensive energy, exergy, economic, and environmental (4E) analysis. *Chem. Eng. J.* **2024**, *491*, 151875.

[36] Tabassum, H.; Mukherjee, S.; Chen, J. J.; Holiharimanana, D.; Karakalos, S.; Yang, X. X.; Hwang, S.; Zhang, T. Y.; Lu, B.; Chen, M. et al. Hydrogen generation via ammonia decomposition on highly efficient and stable Ru-free catalysts: Approaching complete conversion at 450 °C. *Energy Environ. Sci.* **2022**, *15*, 4190–4200.

[37] Mukherjee, S.; Devaguptapu, S. V.; Sviripa, A.; Lund, C. R. F.; Wu, G. Low-temperature ammonia decomposition catalysts for hydrogen generation. *Appl. Catal. B: Environ.* **2018**, *226*, 162–181.

[38] Ramprakash, B.; Lindblad, P.; Eaton-Rye, J. J.; Incharoensakdi, A. current strategies and future perspectives in biological hydrogen production: A review. *Renew. Sustain. Energy Rev.* **2022**, *168*, 112773.

[39] Xia, A.; Cheng, J.; Song, W.; Su, H.; Ding, L.; Lin, R.; Lu, H.; Liu, J.; Zhou, J.; Cen, K. Fermentative hydrogen production using algal biomass as feedstock. *Renew. Sustain. Energy Rev.* **2015**, *51*, 209–230.

[40] Wu, Y. J.; Ghalkhani, M.; Ashrafzadeh Afshar, E.; Karimi, F.; Xia, C. L.; Le, Q. V.; Vasseghian, Y. Recent progress in biomass-derived nanoelectrocatalysts for the sustainable energy development. *Fuel* **2022**, *323*, 124349.

[41] Sharma, M.; Salama, E. S.; Thakur, N.; Alghamdi, H.; Jeon, B. H.; Li, X. K. Advances in the biomass valorization in bioelectrochemical systems: A sustainable approach for microbial-aided electricity and hydrogen production. *Chem. Eng. J.* **2023**, *465*, 142546.

[42] Rueda-Navarro, C. M.; Cabrero-Antonino, M.; Escamilla, P.; Díez-Cabanes, V.; Fan, D.; Atienzar, P.; Ferrer, B.; Vayá, I.; Maurin, G.; Baldoví, H. G. et al. Solar-assisted photocatalytic water splitting using defective UiO-66 solids from modulated synthesis. *Nano Res.* **2024**, *17*, 4134–4150.

[43] Ding, D. F.; Liu, Y. W.; Xia, F. Interface engineering via molecules/ions/groups for electrocatalytic water splitting. *Nano Res.* **2024**, *17*, 7864–7879.

[44] Karthik, P. E.; Rajan, H.; Jothi, V. R.; Sang, B. I.; Yi, S. C. Electronic wastes: A near inexhaustible and an unimaginably wealthy resource for water splitting electrocatalysts. *J. Hazard. Mater.* **2022**, *421*, 126687.

[45] Wang, C. P.; Sun, H.; Bian, G.; Wang, J. X.; Pang, X. X.; Wang, G. Q.; Zhu, J.; Bu, X. H. Electrostatically connected nanoarchitected electrocatalytic films for boosted water splitting. *Nano Res.* **2024**, *17*,

1114–1122.
[46] Iqbal, M. Z.; Zahid, R.; Khan, M. W.; Shaheen, M.; Aziz, U.; Aftab, S. Exploration of catalytically active materials for efficient electrochemical hydrogen and oxygen evolution reactions. *Int. J. Hydrogen Energy* **2023**, *48*, 8045–8070.
[47] Babar, P.; Lokhande, A.; Karade, V.; Pawar, B.; Gang, M. G.; Pawar, S.; Kim, J. H. Bifunctional 2D electrocatalysts of transition metal hydroxide nanosheet arrays for water splitting and urea electrolysis. *ACS Sustain. Chem. Eng.* **2019**, *7*, 10035–10043.
[48] Li, X. P.; Wang, Y.; Wang, J. J.; Da, Y. M.; Zhang, J. F.; Li, L. L.; Zhong, C.; Deng, Y. D.; Han, X. P.; Hu, W. B. Sequential electrodeposition of bifunctional catalytically active structures in MoO_3/Ni–NiO composite electrocatalysts for selective hydrogen and oxygen evolution. *Adv. Mater.* **2020**, *32*, 2003414.
[49] Wang, H. Y.; Chen, L. Y.; Tan, L.; Liu, X. E.; Wen, Y. H.; Hou, W. G.; Zhan, T. R. Electrodeposition of NiFe-layered double hydroxide layer on sulfur-modified nickel molybdate nanorods for highly efficient seawater splitting. *J. Colloid Interface Sci.* **2022**, *613*, 349–358.
[50] Gupta, S.; Patel, M. K.; Miotello, A.; Patel, N. Metal boride-based catalysts for electrochemical water-splitting: A review. *Adv. Funct. Mater.* **2020**, *30*, 1906481.
[51] Han, H. J.; Bai, Z. Y.; Zhang, T.; Wang, X. B.; Yang, X. L.; Ma, X. M.; Zhang, Y. P.; Yang, L.; Lu, J. Hierarchical design and development of nanostructured trifunctional catalysts for electrochemical oxygen and hydrogen reactions. *Nano Energy* **2019**, *56*, 724–732.
[52] Shu, X. X.; Chen, S.; Chen, S.; Pan, W.; Zhang, J. T. Cobalt nitride embedded holey N-doped graphene as advanced bifunctional electrocatalysts for Zn–Air batteries and overall water splitting. *Carbon* **2020**, *157*, 234–243.
[53] Weng, C. C.; Lv, X. W.; Ren, J. T.; Ma, T. Y.; Yuan, Z. Y. Engineering gas-solid-liquid triple-phase interfaces for electrochemical energy conversion reactions. *Electrochem. Energy Rev.* **2022**, *5*, 19.
[54] Huang, Y. Y.; Liu, Q.; Lv, J. Q.; Babu, D. D.; Wang, W. J.; Wu, M. X.; Yuan, D. Q.; Wang, Y. B. Co-intercalation of multiple active units into graphene by pyrolysis of hydrogen-bonded precursors for zinc-air batteries and water splitting. *J. Mater. Chem. A* **2017**, *5*, 20882–20891.
[55] Wu, X. Y.; Han, X. P.; Ma, X. Y.; Zhang, W.; Deng, Y. D.; Zhong, C.; Hu, W. B. Morphology-controllable synthesis of Zn–Co-mixed sulfide nanostructures on carbon fiber paper toward efficient rechargeable zinc-air batteries and water electrolysis. *ACS Appl. Mater. Interfaces* **2017**, *9*, 12574–12583.
[56] Zhang, Y. M.; Yan, R.; Xu, X. H.; He, C.; Zhou, M.; Zeng, Z. Y.; Ma, T.; Wang, M.; Li, S. Next generation noble metal-engineered catalysts: From structure evolution to structure-reactivity correlation in water splitting. *Adv. Funct. Mater.* **2024**, *34*, 2308813.
[57] Liu, D. P.; Zhang, Y. Synergistic photo/electrocatalysis for energy conversion and storage. *Matter* **2021**, *4*, 2678–2680.
[58] Liang, Z. J.; Shen, D.; Wang, L.; Fu, H. G. Recent progress of cobalt-based electrocatalysts for water splitting: Electron modulation, surface reconstitution, and applications. *Nano Res.* **2024**, *17*, 2234–2269.
[59] Liu, W. J.; Jiang, H.; Yu, H. Q. Emerging applications of biochar-based materials for energy storage and conversion. *Energy Environ. Sci.* **2019**, *12*, 1751–1779.
[60] Makinde, W. O.; Hassan, M. A.; Pan, Y.; Guan, G. Q.; López-Salas, N.; Khalil, A. S. G. Sulfur and nitrogen co-doping of peanut shell-derived biochar for sustainable supercapacitor applications. *J. Alloy. Compd.* **2024**, *991*, 174452.
[61] Chen, Q.; Tan, X. F.; Liu, Y. G.; Liu, S. B.; Li, M. F.; Gu, Y. L.; Zhang, P.; Ye, S. J.; Yang, Z. Z.; Yang, Y. Y. Biomass-derived porous graphitic carbon materials for energy and environmental applications. *J. Mater. Chem. A* **2020**, *8*, 5773–5811.
[62] Xiao, R.; Chen, J.; Fu, K.; Zheng, X. Y.; Wang, T.; Zheng, J.; Li, X. G. Hydrolysis batteries: Generating electrical energy during hydrogen absorption. *Angew. Chem., Int. Ed.* **2018**, *57*, 2219–2223.
[63] Gao, Y.; Qiao, Y. H.; Li, X. R.; Huang, C. Y.; Zhang, J.; Wang, Y. R.; Zou, X. L.; Xia, Z. H.; Yang, X. X.; Lu, X. G. et al. Bimetallic site substitution of NiCoP nanoneedles as bifunctional electrocatalyst for boosted water splitting. *Nano Res.* **2024**, *17*, 9540–9549.
[64] Li, T. Y.; Wang, J. J.; Chen, H.; Li, W. C.; Pan, P. Y.; Wu, L. N.; Xu, G.; Chen, H. G. Performance analysis of an integrated biomass-to-energy system based on gasification and pyrolysis. *Energy Convers. Manage.* **2023**, *287*, 117085.
[65] Yu, X.; Mei, J.; Du, Y. S.; Cheng, X. H.; Wang, X.; Wu, Q. Engineered interface of three-dimensional coralliform NiS/FeS_2 heterostructures for robust electrocatalytic water cleavage. *Nano Res.* **2024**, *17*, 4693–4701.
[66] Ghenai, C.; Salameh, T.; Merabet, A. Technico-economic analysis of off grid solar PV/fuel cell energy system for residential community in desert region. *Int. J. Hydrogen Energy* **2020**, *45*, 11460–11470.
[67] Yi, M. J.; Ma, J. Y.; Ren, Y.; Wang, H.; Xie, L.; Zhu, Z. Y.; Zhang, J. H. Ionic Liquid Meets MOF: A Facile Method to Optimize the structure of $CoSe_2$–$NiSe_2$ heterojunctions with N, P, and F triple-doped carbon using ionic liquid for efficient hydrogen evolution and flexible supercapacitors. *Adv. Sci.* **2023**, *10*, 2206029.
[68] Liu, H. P.; Zhu, S. L.; Cui, Z. D.; Li, Z. Y.; Wu, S. L.; Liang, Y. Q. Ni_2P nanoflakes for the high-performing urea oxidation reaction: Linking active sites to a UOR mechanism. *Nanoscale* **2021**, *13*, 1759–1769.
[69] Feng, C.; Faheem, M. B.; Fu, J.; Xiao, Y. Q.; Li, C. L.; Li, Y. B. Fe-based electrocatalysts for oxygen evolution reaction: Progress and perspectives. *ACS Catal.* **2020**, *10*, 4019–4047.
[70] Guo, T. Q.; Li, L. D.; Wang, Z. C. Recent development and future perspectives of amorphous transition metal-based electrocatalysts for oxygen evolution reaction. *Adv. Energy Mater.* **2022**, *12*, 2200827.
[71] Dong, F.; Wu, M. J.; Chen, Z. S.; Liu, X. H.; Zhang, G. X.; Qiao, J. L.; Sun, S. H. Atomically dispersed transition metal-nitrogen-carbon bifunctional oxygen electrocatalysts for zinc-air batteries: Recent advances and future perspectives. *Nano-Micro Lett.* **2022**, *14*, 36.
[72] Hu, C. L.; Zhang, L.; Gong, J. L. Recent progress made in the mechanism comprehension and design of electrocatalysts for alkaline water splitting. *Energy Environ. Sci.* **2019**, *12*, 2620–2645.
[73] Sun, H. M.; Yan, Z. H.; Liu, F. M.; Xu, W. C.; Cheng, F. Y.; Chen, J. Self-supported transition-metal-based electrocatalysts for hydrogen and oxygen evolution. *Adv. Mater.* **2020**, *32*, 1806326.
[74] Ren, S. S.; Duan, X. D.; Liang, S.; Zhang, M. D.; Zheng, H. G. Bifunctional electrocatalysts for Zn-air batteries: Recent developments and future perspectives. *J. Mater. Chem. A* **2020**, *8*, 6144–6182.
[75] Anantharaj, S.; Karthik, P. E.; Subramanian, B.; Kundu, S. Pt nanoparticle anchored molecular self-assemblies of DNA: An extremely stable and efficient HER electrocatalyst with ultralow Pt content. *ACS Catal.* **2016**, *6*, 46604672.
[76] Yu, Z. Y.; Duan, Y.; Feng, X. Y.; Yu, X. X.; Gao, M. R.; Yu, S. H. Clean and affordable hydrogen fuel from alkaline water splitting: Past, recent progress, and future prospects. *Adv. Mater.* **2021**, *33*, 2007100.
[77] Kreuter, W. Electrolysis: The important energy transformer in a world of sustainable energy. *Int. J. Hydrogen Energy* **1998**, *23*, 661–666.
[78] Kazemi, A.; Manteghi, F.; Tehrani Z. Metal electrocatalysts for hydrogen production in water splitting. *ACS Omega* **2024**, *9*, 7310–7335.
[79] Li, Y. H.; Xiao, K.; Huang, C.; Wang, J.; Gao, M.; Hu, A. P.; Tang, Q. L.; Fan, B. B.; Xu, Y. L.; Chen, X. H. Enhanced potassium-ion storage of the 3D carbon superstructure by manipulating the nitrogen-doped species and morphology. *Nano-Micro Lett.* **2021**, *13*, 1.
[80] Fang, Y. H.; Liu, Z. P. Tafel kinetics of electrocatalytic reactions: From experiment to first-principles. *ACS Catal.* **2014**, *4*, 4364–4376.
[81] Duan, H. H.; Li, D. G.; Tang, Y.; He, Y.; Ji, S. F.; Wang, R. Y.; Lv, H. F.; Lopes, P. P.; Paulikas, A. P.; Li, H. Y. et al. High-performance Rh_2P electrocatalyst for efficient water splitting. *J. Am. Chem. Soc.*

2017, *139*, 5494–5502.
[82] Diaz-Morales, O.; Calle-Vallejo, F.; de Munck, C.; Koper, M. T. M. Electrochemical water splitting by gold: Evidence for an oxide decomposition mechanism. *Chem. Sci.* **2013**, *4*, 2334–2343.
[83] Suen, N. T.; Hung, S. F.; Quan, Q.; Zhang, N.; Xu, Y. J.; Chen, H. M. Electrocatalysis for the oxygen evolution reaction: Recent development and future perspectives. *Chem. Soc. Rev.* **2017**, *46*, 337–365.
[84] Ledendecker, M.; Krick Calderón, S.; Papp, C.; Steinrück, H. P.; Antonietti, M.; Shalom, M. The synthesis of nanostructured Ni_5P_4 films and their use as a non-noble bifunctional electrocatalyst for full water splitting. *Angew. Chem., Int. Ed.* **2015**, *54*, 12361–12365.
[85] Liu, J. Y.; Duan, S.; Shi, H.; Wang, T. Y.; Yang, X. X.; Huang, Y. H.; Wu, G.; Li, Q. Rationally designing efficient electrocatalysts for direct seawater splitting: Challenges, achievements, and promises. *Angew. Chem., Int. Ed.* **2022**, *61*, e202210753.
[86] Wang, J.; Liao, T.; Wei, Z. Z.; Sun, J. T.; Guo, J. J.; Sun, Z. Q. Heteroatom-doping of non-noble metal-based catalysts for electrocatalytic hydrogen evolution: An electronic structure tuning strategy. *Small Methods* **2021**, *5*, 2000988.
[87] Xu, H.; Zhao, Y. T.; He, G. Y.; Chen, H. Q. Race on engineering noble metal single-atom electrocatalysts for water splitting. *Int. J. Hydrogen Energy* **2022**, *47*, 14257–14279.
[88] Li, X. P.; Huang, C.; Han, W. K.; Ouyang, T.; Liu, Z. Q. Transition metal-based electrocatalysts for overall water splitting. *Chin. Chem. Lett.* **2021**, *32*, 2597–2616.
[89] Yan, Y.; Xia, B. Y.; Zhao, B.; Wang, X. A review on noble-metal-free bifunctional heterogeneous catalysts for overall electrochemical water splitting. *J. Mater. Chem. A* **2016**, *4*, 17587–17603.
[90] Jamesh, M. I.; Harb, M. Tuning the electronic structure of the earth-abundant electrocatalysts for oxygen evolution reaction (OER) to achieve efficient alkaline water splitting-A review. *J. Energy Chem.* **2021**, *56*, 299–342.
[91] Mohammed-Ibrahim, J. A review on NiFe-based electrocatalysts for efficient alkaline oxygen evolution reaction. *J. Power Sources* **2020**, *448*, 227375.
[92] Yuan, H. F.; Wang, S. M.; Ma, Z. Z.; Kundu, M.; Tang, B.; Li, J. P.; Wang, X. G. Oxygen vacancies engineered self-supported b doped Co_3O_4 nanowires as an efficient multifunctional catalyst for electrochemical water splitting and hydrolysis of sodium borohydride. *Chem. Eng. J.* **2021**, *404*, 126474.
[93] Han, X. P.; Wu, X. Y.; Deng, Y. D.; Liu, J.; Lu, J.; Zhong, C.; Hu, W. B. Ultrafine Pt Nanoparticle-decorated pyrite-type CoS_2 nanosheet arrays coated on carbon cloth as a bifunctional electrode for overall water splitting. *Adv. Energy Mater.* **2018**, *8*, 1800935.
[94] Jiang, H. L.; Qin, H. L.; Zhou, P.; Kong, L. R.; Wang, C. D.; Ji, Z. Y.; Shen, X. P.; Zhu, G. X.; Yuan, A. H. Partial sulfidation strategy to NiCo-LDH@NiCoS coupled with NiFe-LDH for highly efficient overall water splitting. *Int. J. Hydrogen Energy* **2024**, *58*, 892–901.
[95] Deng, J.; Ren, P. J.; Deng, D. H.; Yu, L.; Yang, F.; Bao, X. H. Highly active and durable non-precious-metal catalysts encapsulated in carbon nanotubes for hydrogen evolution reaction. *Energy Environ. Sci.* **2014**, *7*, 1919–1923.
[96] Long, X.; Li, G. X.; Wang, Z. L.; Zhu, H. Y.; Zhang, T.; Xiao, S.; Guo, W. Y.; Yang, S. H. Metallic iron-nickel sulfide ultrathin nanosheets as a highly active electrocatalyst for hydrogen evolution reaction in acidic media. *J. Am. Chem. Soc.* **2015**, *137*, 11900–11903.
[97] Kuang, Y.; Feng, G.; Li, P. S.; Bi, Y. M.; Li, Y. P.; Sun, X. M. Single-crystalline ultrathin nickel nanosheets array from *in situ* topotactic reduction for active and stable electrocatalysis. *Angew. Chem., Int. Ed.* **2016**, *55*, 693–697.
[98] Wang, Y. H.; Zhang, G. X.; Xu, W. W.; Wan, P. B.; Lu, Z. Y.; Li, Y. P.; Sun, X. M. A 3D nanoporous Ni–Mo electrocatalyst with negligible overpotential for alkaline hydrogen evolution. *ChemElectroChem* **2014**, *1*, 1138–1144.
[99] Jamesh, M. I. Recent progress on earth abundant hydrogen evolution reaction and oxygen evolution reaction bifunctional electrocatalyst for overall water splitting in alkaline media. *J. Power Sources* **2016**, *333*, 213–236.
[100] Zhang, K.; Duan, Y. X.; Graham, N.; Yu, W. Z. Unveiling the synergy of polymorph heterointerface and sulfur vacancy in NiS/Ni_3S_2 electrocatalyst to promote alkaline hydrogen evolution reaction. *Appl. Catal. B: Environ.* **2023**, *323*, 122144.
[101] Wang, M.; Yang, H.; Shi, J. N.; Chen, Y. F.; Zhou, Y.; Wang, L. G.; Di, S. J.; Zhao, X.; Zhong, J.; Cheng, T. et al. Alloying nickel with molybdenum significantly accelerates alkaline hydrogen electrocatalysis. *Angew. Chem., Int. Ed.* **2021**, *60*, 5771–5777.
[102] Wang, D. D.; Liu, Y.; Liu, L. L.; Shan, D. F.; Shen, G. X.; Peng, S. L.; Zhang, H.; Wang, X. D. Biomimetic three-dimensional multilevel nanoarray electrodes with superaerophobicity as efficient bifunctional catalysts for electrochemical water splitting. *Nano Res.* **2023**, *16*, 6584–6592.
[103] Wang, J. S.; Xin, S. S.; Xiao, Y.; Zhang, Z. F.; Li, Z. M.; Zhang, W.; Li, C. J.; Bao, R.; Peng, J.; Yi, J. H. et al. Manipulating the water dissociation electrocatalytic sites of bimetallic nickel-based alloys for highly efficient alkaline hydrogen evolution. *Angew. Chem., Int. Ed.* **2022**, *61*, e202202518.
[104] Yu, W. L.; Liu, H. R.; Zhao, Y.; Fu, Y. L.; Xiao, W. P.; Dong, B.; Wu, Z. X.; Chai, Y. M.; Wang, L. Amorphous NiO_n coupled with trace PtO_x toward superior electrocatalytic overall water splitting in alkaline seawater media. *Nano Res.* **2023**, *16*, 6517–6530.
[105] Lai, W. H.; Zhang, L. F.; Hua, W. B.; Indris, S.; Yan, Z. C.; Hu, Z.; Zhang, B. W.; Liu, Y. N.; Wang, L.; Liu, M. et al. General π-electron-assisted strategy for Ir, Pt, Ru, Pd, Fe, Ni single-atom electrocatalysts with bifunctional active sites for highly efficient water splitting. *Angew. Chem., Int. Ed.* **2019**, *58*, 11868–11873.
[106] Skúlason, E.; Tripkovic, V.; Björketun, M. E.; Gudmundsdóttir, S.; Karlberg, G.; Rossmeisl, J.; Bligaard, T.; Jónsson, H.; Nørskov, J. K. Modeling the electrochemical hydrogen oxidation and evolution reactions on the basis of density functional theory calculations. *J. Phys. Chem. C* **2010**, *114*, 181823–18197.
[107] Fan, Y. X.; Li, L.; Yu, G.; Geng, D. C.; Zhang, X. T.; Hu, W. P. Recent advances in growth of large-sized 2D single crystals on Cu substrates. *Adv. Mater.* **2021**, *33*, 2003956.
[108] Sun, H. N.; Xu, X. M.; Kim, H.; Jung, W.; Zhou, W.; Shao, Z. P. Electrochemical water splitting: Bridging the gaps between fundamental research and industrial applications. *Energy Environ. Mater.* **2023**, *6*, e12441.
[109] Chen, J.; Zhang, L. C.; Li, J.; He, X.; Zheng, Y. Y.; Sun, S. J.; Fang, X. D.; Zheng, D. D.; Luo, Y. S.; Wang, Y. et al. High-efficiency overall alkaline seawater splitting: Using a nickel-iron sulfide nanosheet array as a bifunctional electrocatalyst. *J. Mater. Chem. A* **2023**, *11*, 1116–1122.
[110] Suryanto, B. H. R.; Wang, Y.; Hocking, R. K.; Adamson, W.; Zhao, C. Overall electrochemical splitting of water at the heterogeneous interface of nickel and iron oxide. *Nat. Commun.* **2019**, *10*, 5599.
[111] Kuang, Y.; Kenney, M. J.; Meng, Y. T.; Hung, W. H.; Liu, Y. J.; Huang, J. E.; Prasanna, R.; Li, P. S.; Li, Y. P.; Wang, L. et al. Solar-driven, highly sustained splitting of seawater into hydrogen and oxygen fuels. *Proc. Natl. Acad. Sci. USA* **2019**, *116*, 6624–6629.
[112] Zhao, M.; Li, W.; Li, J. Y.; Hu, W. H.; Li, C. M. Strong electronic interaction enhanced electrocatalysis of metal sulfide clusters embedded metal-organic framework ultrathin nanosheets toward highly efficient overall water splitting. *Adv. Sci.* **2020**, *7*, 2001965.
[113] Fei, B.; Chen, Z. L.; Liu, J. X.; Xu, H. B.; Yan, X. X.; Qing, H. L.; Chen, M.; Wu, R. B. Ultrathinning nickel sulfide with modulated electron density for efficient water splitting. *Adv. Energy Mater.* **2020**, *10*, 2001963.
[114] Hu, L. Y.; Zeng, X.; Wei, X. Q.; Wang, H. J.; Wu, Y.; Gu, W. L.; Shi, L.; Zhu, C. Z. Interface engineering for enhancing electrocatalytic oxygen evolution of NiFe LDH/NiTe heterostructures. *Appl. Catal. B: Environ.* **2020**, *273*, 119014.
[115] Man, I. C.; Su, H. -Y.; Calle-Vallejo, F.; Hansen, H. A.; Martínez, J. I.; Inoglu, N. G.; Kitchin, J.; Jaramillo, T. F.; Nørskov, J. K.; Rossmeisl, J. Universality in oxygen evolution electrocatalysis on

oxide surfaces. *ChemCatChem* **2011**, *3*, 1159–1165.
[116] Du, Y. M.; Li, B.; Xu, G. R.; Wang, L. Recent advances in interface engineering strategy for highly-efficient electrocatalytic water splitting. *InfoMat* **2023**, *5*, e12377.
[117] Qin, C. L.; Chen, S.; Gomaa, H.; Shenashen, M. A.; El-Safty, S. A.; Liu, Q.; An, C. H.; Liu, X. J.; Deng, Q. B.; Hu, N. Regulating HER and OER performances of 2D materials by the external physical fields. *Acta Phys. Chim. Sin.* **2024**, *40*, ©2307059.
[118] Yan, Y. T.; Lin, J. H.; Huang, K. K.; Zheng, X. H.; Qiao, L.; Liu, S. D.; Cao, J.; Jun, S. C.; Yamauchi, Y.; Qi, J. L. Tensile strain-mediated spinel ferrites enable superior oxygen evolution activity. *J. Am. Chem. Soc.* **2023**, *145*, 24218–24229.
[119] Zhou, S. H.; Shi, L.; Li, Y. Z.; Yang, T.; Zhao, S. L. Metal-organic framework-based electrocatalysts for acidic water splitting. *Adv. Funct. Mater.* **2024**, *34*, 2400767.
[120] Zhang, K. X.; Zou, R. Q. Advanced transition metal-based oer electrocatalysts: Current status, opportunities, and challenges. *Small* **2021**, *17*, 2100129.
[121] Lu, Y. X.; Dong, C. L.; Huang, Y. C.; Zou, Y. Q.; Liu, Z. J.; Liu, Y. B.; Li, Y. Y.; He, N. H.; Shi, J. Q.; Wang, S. Y. Identifying the geometric site dependence of spinel oxides for the electrooxidation of 5-hydroxymethylfurfural. *Angew. Chem., Int. Ed.* **2020**, *59*, 19215–19221.
[122] Cheng, Q. L.; Pang, J. B.; Sun, D. H.; Wang, J. G.; Zhang, S.; Liu, F.; Chen, Y. K.; Yang, R. Q.; Liang, N.; Lu, X. H. et al. WSe_2 2D p-type semiconductor-based electronic devices for information technology: Design, preparation, and applications. *InfoMat* **2020**, *2*, 656–697.
[123] Zhu, P. C.; Mu, S. R.; Huang, W. H.; Sun, Z. Y.; Lin, Y. Y.; Chen, K.; Pan, Z. F.; Haghighi, M. G.; Sedghi, R.; Wang, J. L. et al. Soft multifunctional neurological electronic skin through intrinsically stretchable synaptic transistor. *Nano Res.* **2024**, *17*, 6550–6559.
[124] Bruix, A.; Rodriguez, J. A.; Ramírez, P. J.; Senanayake, S. D.; Evans, J.; Park, J. B.; Stacchiola, D.; Liu, P.; Hrbek, J.; Illas, F. A new type of strong metal-support interaction and the production of H_2 through the transformation of water on Pt/CeO_2 (111) and Pt/CeO_x /TiO_2 (110) catalysts. *J. Am. Chem. Soc.* **2012**, *134*, 8968–8974.
[125] Song, Q.; Qiao, X. Z.; Liu, L. Z.; Xue, Z. J.; Huang, C. H.; Wang, T. Ruthenium@N-doped graphite carbon derived from carbon foam for efficient hydrogen evolution reaction. *Chem. Commun.* **2019**, *55*, 965–968.
[126] Mu, X. Q.; Yu, M. Y.; Liu, X. Y.; Liao, Y. R.; Chen, F. J.; Pan, H. Z.; Chen, Z. Y.; Liu, S. L.; Wang, D. S.; Mu, S. C. High-entropy ultrathin amorphous metal-organic framework-stabilized Ru(Mo) dual-atom sites for water oxidation. *ACS Energy Lett.* **2024**, *9*, 5763–5770.
[127] Li, Y. Q.; Liu, X.; Xu, J. L.; Chen, S. R. Ruthenium-based electrocatalysts for hydrogen evolution reaction: From nanoparticles to single atoms. *Small* **2024**, *20*, 2402846.
[128] Liu, Z. L.; Li, B. Q.; Feng, Y. J.; Jia, D. C.; Li, C. C.; Sun, Q. F.; Zhou, Y. Strong electron coupling of Ru and vacancy-rich carbon dots for synergistically enhanced hydrogen evolution reaction. *Small* **2021**, *17*, 2102496.
[129] Che, Z. W.; Lu, X. Y.; Cai, B. F.; Xu, X. X.; Bao, J. C.; Liu, Y. Ligand-controlled synthesis of high density and ultra-small Ru nanoparticles with excellent electrocatalytic hydrogen evolution performance. *Nano Res.* **2022**, *15*, 1269–1275.
[130] Jiang, A. N.; Wang, Z. G.; Li, Q.; Dong, M. D. An efficient ruthenium-based dual-electrocatalyst towards hydrogen evolution and oxygen reduction reactions. *Mater. Today Phys.* **2021**, *16*, 100300.
[131] Kang, X.; Yang, F. N.; Zhang, Z. Y.; Liu, H. M.; Ge, S. Y.; Hu, S. Q.; Li, S. H.; Luo, Y. T.; Yu, Q. M.; Liu, Z. B. et al. A corrosion-resistant RuMoNi catalyst for efficient and long-lasting seawater oxidation and anion exchange membrane electrolyzer. *Nat. Commun.* **2023**, *14*, 3607.
[132] Mu, X. Q.; Zhang, X. Y.; Chen, Z. Y.; Gao, Y.; Yu, M.; Chen, D.; Pan, H. Z.; Liu, S. L.; Wang, D. S.; Mu, S. C. Constructing symmetry-mismatched $Ru_xFe_{3-x}O_4$ heterointerface-supported Ru clusters for efficient hydrogen evolution and oxidation reactions. *Nano Lett.* **2024**, *24*, 1015–1023.
[133] Cheng, H. F.; Yang, N. L.; Lu, Q. P.; Zhang, Z. C.; Zhang, H. Syntheses and properties of metal nanomaterials with novel crystal phases. *Adv. Mater.* **2018**, *30*, 1707189.
[134] Zheng, Y.; Jiao, Y.; Zhu, Y. H.; Li, L. H.; Han, Y.; Chen, Y.; Jaroniec, M.; Qiao, S. Z. High electrocatalytic hydrogen evolution activity of an anomalous ruthenium catalyst. *J. Am. Chem. Soc.* **2016**, *138*, 16174–16181.
[135] Zhao, M.; Chen, Z. T.; Lyu, Z. H.; Hood, Z. D.; Xie, M. H.; Vara, M.; Chi, M. F.; Xia, Y. N. Ru octahedral nanocrystals with a face-centered cubic structure, {111} facets, thermal stability up to 400 °C, and enhanced catalytic activity. *J. Am. Chem. Soc.* **2019**, *141*, 7028–7036.
[136] Liu, Z. Q.; Nie, K. K.; Qu, X. Y.; Li, X. H.; Li, B. J.; Yuan, Y. L.; Chong, S. K.; Liu, P.; Li, Y. G.; Yin, Z. Y. et al. General bottom-up colloidal synthesis of nano-monolayer transition-metal dichalcogenides with high 1T′-phase purity. *J. Am. Chem. Soc.* **2022**, *144*, 4863–4873.
[137] Cao, F. C.; Zhang, Y.; Wang, H. Q.; Khan, K.; Tareen, A. K.; Qian, W. J.; Zhang, H.; Agren, H. Recent advances in oxidation stable chemistry of 2D MXenes. *Adv. Mater.* **2022**, *34*, 2107554.
[138] Chang, C.; Chen, W.; Chen, Y.; Chen, Y. H.; Chen, Y.; Ding, F.; Fan, C. H.; Fan, H. J.; Fan, Z. X.; Gong, C. et al. Recent progress on two-dimensional materials. *Acta Phys. Chim. Sin.* **2021**, *37*, 2108017.
[139] Samadi, M.; Sarikhani, N.; Zirak, M.; Zhang, H.; Zhang, H. L.; Moshfegh, A. Z. Group 6 transition metal dichalcogenide nanomaterials: Synthesis, applications and future perspectives. *Nanoscale Horiz.* **2018**, *3*, 90–204.
[140] Luo, Y.; Yang, X. F.; Wang, C. H.; Fraser, A.; Zhang, H. Z.; Sun, X. L.; Li, X. F. Advanced metal anodes and their interface design toward safe metal batteries: A comprehensive review. *Prog. Mater. Sci.* **2023**, *139*, 101171.
[141] Li, Y. P.; Niu, S. W.; Liu, P. G.; Pan, R. R.; Zhang, H. K.; Ahmad, N.; Shi, Y.; Liang, X.; Cheng, M. Y.; Chen, S. H. et al. Ruthenium nanoclusters and single atoms on α-MoC/N-doped carbon achieves low-input/input-free hydrogen evolution via decoupled/coupled hydrazine oxidation. *Angew. Chem., Int. Ed.* **2024**, *63*, e202316755.
[142] Guo, Y. J.; Liu, Z. Y.; Zhou, D. Y.; Zhang, M. Y.; Zhang, Y.; Li, R. Z.; Liu, S. L.; Wang, D. S.; Dai, Z. H. Competition and synergistic effects of Ru-based single-atom and cluster catalysts in electrocatalytic reactions. *Sci. China Mater.* **2024**, *67*, 1706–1720.
[143] Bao, M. J.; Amiinu, I. S.; Peng, T.; Li, W. Q.; Liu, S. J.; Wang, Z.; Pu, Z. H.; He, D. P.; Xiong, Y. L.; Mu, S. C. Surface evolution of PtCu alloy shell over Pd nanocrystals leads to superior hydrogen evolution and oxygen reduction reactions. *ACS Energy Lett.* **2018**, *3*, 940–945.
[144] Wei, M.; Sun, Y. Y.; Zhang, J. Y.; Ai, F.; Xi, S. B.; Wang, J. K. High-entropy alloy nanocrystal assembled by nanosheets with d–d electron interaction for hydrogen evolution reaction. *Energy Environ. Sci.* **2023**, *16*, 4009–4019.
[145] Liu, G. G.; Zhou, W.; Ji, Y. R.; Chen, B.; Fu, G. T.; Yun, Q. B.; Chen, S. M.; Lin, Y. X.; Yin, P. F.; Cui, X. Y. et al. Hydrogen-intercalation-induced lattice expansion of Pd@Pt core-shell nanoparticles for highly efficient electrocatalytic alcohol oxidation. *J. Am. Chem. Soc.* **2021**, *143*, 11262–11270.
[146] Qin, Y. L.; Yu, K. D.; Wang, G.; Zhuang, Z. C.; Dou, Y. H.; Wang, D. S.; Chen, Z. B. Adjacent-ligand tuning of atomically precise Cu−Pd sites enables efficient methanol electrooxidation with a CO-free pathway. *Angew. Chem., Int. Ed.* **2025**, *64*, e202420817.
[147] Zhang, Y.; Mu, X. Q.; Liu, Z. Y.; Zhao, H. Y.; Zhuang, Z. C.; Zhang, Y. F.; Mu, S. C.; Liu, S. L.; Wang, D. S.; Dai, Z. H. Twin-distortion modulated ultra-low coordination PtRuNi-O_x catalyst for enhanced

hydrogen production from chemical wastewater. *Nat. Commun.* **2024**, *15*, 10149.
[148] Mu, X. Q.; Yuan, Y. T.; Yu, M.; Hu, Y. J.; Zeng, W. H.; Peng, W.; Zhang, Y. F.; Liu, X. Y.; Liu, S. L.; Mu, S. C. Robust water/seawater-electrolysis hydrogen production at industrial-scale current densities by modulating built-in-outer electric field of catalytic substance. *Nano Energy* **2024**, *131*, 110216.
[149] Li, K.; Li, Y.; Wang, Y. M.; Ge, J. J.; Liu, C. P.; Xing, W. Enhanced electrocatalytic performance for the hydrogen evolution reaction through surface enrichment of platinum nanoclusters alloying with ruthenium *in situ* embedded in carbon. *Energy Environ. Sci.* **2018**, *11*, 1232–1239.
[150] Guo, S. H.; Wang, E. K. Noble metal nanomaterials: Controllable synthesis and application in fuel cells and analytical sensors. *Nano Today* **2011**, *6*, 240–264.
[151] Shao, Q.; Lu, K. Y.; Huang, X. Q. Platinum group nanowires for efficient electrocatalysis. *Small Methods* **2019**, *3*, 1800545.
[152] Pedersen, A. F.; Ulrikkeholm, E. T.; Escudero-Escribano, M.; Johansson, T. P.; Malacrida, P.; Pedersen, C. M.; Hansen, M. H.; Jensen, K. D.; Rossmeisl, J.; Friebel, D. et al. Probing the nanoscale structure of the catalytically active overlayer on Pt alloys with rare earths. *Nano Energy* **2016**, *29*, 249–260.
[153] Mu, X. Q.; Gu, J. N.; Feng, F. Y.; Xiao, Z. Y.; Chen, C. Y.; Liu, S. L.; Mu, S. C. RuRh bimetallene nanoring as high-efficiency pH-universal catalyst for hydrogen evolution reaction. *Adv. Sci.* **2021**, *8*, 2002341.
[154] He, J.; Zhou, X.; Xu, P.; Sun, J. M. Regulating electron redistribution of intermetallic iridium oxide by incorporating Ru for efficient acidic water oxidation. *Adv. Energy Mater.* **2021**, *11*, 2102883.
[155] Li, H. Y.; Tang, Q. W.; He, B. L.; Yang, P. Z. Robust electrocatalysts from an alloyed Pt–Ru–M (M = Cr, Fe, Co, Ni, Mo)-decorated Ti mesh for hydrogen evolution by seawater splitting. *J. Mater. Chem. A* **2016**, *4*, 6513–6520.
[156] Niu, X. M.; Tang, Q. W.; He, B. L.; Yang, P. Z. Robust and stable ruthenium alloy electrocatalysts for hydrogen evolution by seawater splitting. *Electrochim. Acta* **2016**, *208*, 180–187.
[157] Hao, J. C.; Zhuang, Z. C.; Cao, K. C.; Gao, G. H.; Wang, C.; Lai, F. L.; Lu, S. L.; Ma, P. M.; Dong, W. F.; Liu, T. X. et al. Unraveling the electronegativity-dominated intermediate adsorption on high-entropy alloy electrocatalysts. *Nat. Commun.* **2022**, *13*, 2662.
[158] Löffler, T.; Ludwig, A.; Rossmeisl, J.; Schuhmann, W. What makes high-entropy alloys exceptional electrocatalysts. *Angew. Chem., Int. Ed.* **2021**, *60*, 26894–26903.
[159] Chen, Y.; Lin, J.; Jia, B. H.; Wang, X. D.; Jiang, S. Y.; Ma, T. Y. Isolating single and few atoms for enhanced catalysis. *Adv. Mater.* **2022**, *34*, 2201796.
[160] Yang, J. R.; Zhu, C. X.; Wang, D. S. A simple organo-electrocatalysis system for the chlor-related industry. *Angew. Chem., Int. Ed.* **2024**, *63*, e202406883.
[161] Campbell, C. T. Electronic perturbations. *Nat. Chem.* **2012**, *4*, 597–598.
[162] Lyu, S. L.; Guo, C. X.; Wang, J. N.; Li, Z. J.; Yang, B.; Lei, L. C.; Wang, L. P.; Xiao, J. P.; Zhang, T.; Hou, Y. Exceptional catalytic activity of oxygen evolution reaction via two-dimensional graphene multilayer confined metal-organic frameworks. *Nat. Commun.* **2022**, *13*, 6171.
[163] He, F.; Zheng, Q.; Yang, X. X.; Wang, L. G.; Zhao, Z. L.; Xu, Y. K.; Hu, L. Z.; Kuang, Y. B.; Yang, B.; Li, Z. J. et al. Spin-state modulation on metal-organic frameworks for electrocatalytic oxygen evolution. *Adv. Mater.* **2023**, *35*, 2304022.
[164] Liu, Y.; Yang, Y. P.; Peng, Z. K.; Liu, Z. Y.; Chen, Z. M.; Shang, L.; Lu, S. Y.; Zhang, T. R. Self-crosslinking carbon dots loaded ruthenium dots as an efficient and super-stable hydrogen production electrocatalyst at all pH values. *Nano Energy* **2019**, *65*, 104023.
[165] Li, W. D.; Wei, Z. H.; Wang, B. Y.; Liu, Y.; Song, H. Q.; Tang, Z. Y.; Yang, B.; Lu, S. Y. Carbon quantum dots enhanced the activity for the hydrogen evolution reaction in ruthenium-based electrocatalysts. *Mater. Chem. Front.* **2020**, *4*, 277–284.
[166] Song, H. Q.; Wu, M.; Tang, Z. Y.; Tse, J. S.; Yang, B.; Lu, S. Y. Single atom ruthenium-doped CoP/CdS nanosheets via splicing of carbon-dots for robust hydrogen production. *Angew. Chem., Int. Ed.* **2021**, *60*, 7234–7244.
[167] Kweon, D. H.; Okyay, M. S.; Kim, S. J.; Jeon, J. P.; Noh, H. J.; Park, N.; Mahmood, J.; Baek, J. B. Ruthenium anchored on carbon nanotube electrocatalyst for hydrogen production with enhanced faradaic efficiency. *Nat. Commun.* **2020**, *11*, 1278.
[168] Liang, Q. R.; Li, Q. Z.; Xie, L.; Zeng, H.; Zhou, S.; Huang, Y. N.; Yan, M.; Zhang, X.; Liu, T. Y.; Zeng, J. et al. Superassembly of surface-enriched Ru nanoclusters from trapping-bonding strategy for efficient hydrogen evolution. *ACS Nano* **2022**, *16*, 7993–8004.
[169] Ju, Q. J.; Ma, R. G.; Pei, Y.; Guo, B. B.; Li, Z. C.; Liu, Q.; Thomas, T.; Yang, M. H.; Hutchings, G. J.; Wang, J. C. Ruthenium triazine composite: A good match for increasing hydrogen evolution activity through contact electrification. *Adv. Energy Mater.* **2020**, *10*, 2000067.
[170] Sun, Y. M.; Xue, Z. Q.; Liu, Q. L.; Jia, Y. L.; Li, Y. L.; Liu, K.; Lin, Y. Y.; Liu, M.; Li, G. Q.; Su, C. Y. Modulating electronic structure of metal-organic frameworks by introducing atomically dispersed Ru for efficient hydrogen evolution. *Nat. Commun.* **2021**, *12*, 1369.
[171] Wang, Q. L.; Xu, C. Q.; Liu, W.; Hung, S. F.; Bin Yang, H.; Gao, J. J.; Cai, W. Z.; Chen, H. M.; Li, J.; Liu, B. Coordination engineering of iridium nanocluster bifunctional electrocatalyst for highly efficient and pH-universal overall water splitting. *Nat. Commun.* **2020**, *11*, 4246.
[172] Kuang, P. Y.; Wang, Y. R.; Zhu, B. C.; Xia, F. J.; Tung, C. W.; Wu, J. S.; Chen, H. M.; Yu, J. G. Pt single atoms supported on N-doped mesoporous hollow carbon spheres with enhanced electrocatalytic H_2-evolution activity. *Adv. Mater.* **2021**, *33*, 2008599.
[173] Hu, Y. M.; Chao, T. T.; Li, Y. P.; Liu, P. G.; Zhao, T. H.; Yu, G.; Chen, C.; Liang, X.; Jin, H. L.; Niu, S. W. et al. Cooperative Ni(Co)–Ru–P sites activate dehydrogenation for hydrazine oxidation assisting self-powered H_2 production. *Angew. Chem., Int. Ed.* **2023**, *62*, e202308800.
[174] Meng, W. X.; Pang, R.; Li, M.; Han, L.; Kong, X. B.; Zhang, D.; Zhang, S. P.; Zhang, Y. J.; Shang, Y. Y.; Cao, A. Y. Integrated catalyst-substrate electrodes for electrochemical water splitting: A review on dimensional engineering strategy. *Small* **2024**, *21*, 2310469.
[175] Tong, Y.; Chen, P. Z. Nanostructure engineering of ruthenium-modified electrocatalysts for efficient electrocatalytic water splitting. *J. Mater. Chem. A* **2024**, *12*, 3844–3878.
[176] Wang, Y. B.; Jiang, Y.; Zhao, Y. X.; Ge, X. L.; Lu, Q.; Zhang, T.; Xie, D. S.; Li, M.; Bu, Y. F. Design strategies of perovskite nanofibers electrocatalysts for water splitting: A mini review. *Chem. Eng. J.* **2023**, *451*, 138710.
[177] Zhai, P. L.; Zhang, Y. X.; Wu, Y. Z.; Gao, J. F.; Zhang, B.; Cao, S. Y.; Zhang, Y. T.; Li, Z. W.; Sun, L. C.; Hou, J. G. Engineering active sites on hierarchical transition bimetal oxides/sulfides heterostructure array enabling robust overall water splitting. *Nat. Commun.* **2020**, *11*, 5462.
[178] Gao, Y.; Yang, C. D.; Sun, F. L.; He, D. P.; Wang, X. Q.; Chen, J.; Zheng, X. B.; Liu, R. C.; Pan, H. G.; Wang, D. S. Ligand-tuning metallic sites in molecular complexes for efficient water oxidation. *Angew. Chem., Int. Ed.* **2025**, *64*, e202415755.
[179] Jiao, S. L.; Fu, X. W.; Ruan, S. C.; Zeng, Y. J.; Huang, H. W. Breaking the periodic arrangement of atoms for the enhanced electrochemical reduction of nitrogen and water oxidation. *Sci. China Mater.* **2022**, *65*, 147–154.
[180] Lu, Z. Y.; Chen, G. X.; Siahrostami, S.; Chen, Z. H.; Liu, K.; Xie, J.; Liao, L.; Wu, T.; Lin, D. C.; Liu, Y. Y. et al. High-efficiency oxygen reduction to hydrogen peroxide catalysed by oxidized carbon materials. *Nat. Catal.* **2018**, *1*, 156–162.
[181] Ma, M.; Li, G.; Yan, W.; Wu, Z. Z.; Zheng, Z. P.; Zhang, X. B.; Wang, Q. X.; Du, G. F.; Liu, D. Y.; Xie, Z. X. et al. Single-atom molybdenum engineered platinum nanocatalyst for boosted alkaline

hydrogen oxidation. *Adv. Energy Mater.* **2022**, *12*, 2103336.
[182] Jiang, Y. Y.; Ni, P. J.; Chen, C. X.; Lu, Y. Z.; Yang, P.; Kong, B.; Fisher, A.; Wang, X. Selective electrochemical H_2O_2 production through two-electron oxygen electrochemistry. *Adv. Energy Mater.* **2018**, *8*, 1801909.
[183] Chen, Y. M.; Zhang, L.; Yang, Y.; Pang, B.; Xu, W. H.; Duan, G. G.; Jiang, S. H.; Zhang, K. Recent progress on nanocellulose aerogels: Preparation, modification, composite fabrication, applications. *Adv. Mater.* **2021**, *33*, 2005569.
[184] Shen, Z. H.; Qin, M. L.; Xiong, F.; Zou, R. Q.; Zhang, J. Nanocellulose-based composite phase change materials for thermal energy storage: Status and challenges. *Energy Environ. Sci.* **2023**, *16*, 830–861.
[185] Niu, Y. T.; Li, F. Z.; Zhao, W. X.; Cheng, W. Fabrication and application of macroscopic nanowire aerogels. *Nanoscale* **2021**, *13*, 7430–7446.
[186] Zeng, Z. H.; Wu, T. T.; Han, D. X.; Ren, Q.; Siqueira, G.; Nyström, G. Ultralight, flexible, and biomimetic nanocellulose/silver nanowire aerogels for electromagnetic interference shielding. *ACS Nano* **2020**, *14*, 2927–2938.
[187] Du, R.; Wang, J. Y.; Wang, Y.; Hübner, R.; Fan, X. L.; Senkovska, I.; Hu, Y.; Kaskel, S.; Eychmüller, A. Unveiling reductant chemistry in fabricating noble metal aerogels for superior oxygen evolution and ethanol oxidation. *Nat. Commun.* **2020**, *11*, 1590.
[188] Yu, R.; Cao, X.; Chen, Q. Q.; Li, W. J.; Huang, A. J.; Wei, X. W.; Mao, J. J. D-band center optimization of edge-rich ultrathin RuZn nanosheets with moiré superlattices for pH-universal hydrogen evolution reaction. *Small* **2023**, *19*, 2303440.
[189] Zhang, J. C.; Chen, G. B.; Liu, Q. C.; Fan, C.; Sun, D. M.; Tang, Y. W.; Sun, H. J.; Feng, X. L. Competitive adsorption: Reducing the poisoning effect of adsorbed hydroxyl on Ru single-atom site with SnO_2 for efficient hydrogen evolution. *Angew. Chem., Int. Ed.* **2022**, *61*, e202209486.
[190] Huang, X. X.; Lu, R. H.; Cen, Y. P.; Wang, D. C.; Jin, S.; Chen, W. X.; Geoffrey, I.; Waterhouse, N.; Wang, Z. Y.; Tian, S. B. et al. Micropore-confined Ru nanoclusters catalyst for efficient pH-universal hydrogen evolution reaction. *Nano Res.* **2023**, *16*, 9073–9080.
[191] Cao, L. L.; Luo, Q. Q.; Chen, J. J.; Wang, L.; Lin, Y.; Wang, H. J.; Liu, X. K.; Shen, X. Y.; Zhang, W.; Liu, W. et al. Dynamic oxygen adsorption on single-atomic ruthenium catalyst with high performance for acidic oxygen evolution reaction. *Nat. Commun.* **2019**, *10*, 4849.
[192] Fan, R. Y.; Zhang, Y. S.; Lv, J. Y.; Han, G. Q.; Chai, Y. M.; Dong, B. The promising seesaw relationship between activity and stability of Ru-based electrocatalysts for acid oxygen evolution and proton exchange membrane water electrolysis. *Small* **2024**, *20*, 2304636.
[193] Xiao, M. L.; Gao, L. Q.; Wang, Y.; Wang, X.; Zhu, J. B.; Jin, Z.; Liu, C. P.; Chen, H. Q.; Li, G. R.; Ge, J. J. et al. Engineering energy level of metal center: Ru single-atom site for efficient and durable oxygen reduction catalysis, *J. Am. Chem. Soc.* **2019**, *141*, 19800–19806.
[194] He, Q.; Zhou, Y. Z.; Shou, H. W.; Wang, X. Y.; Zhang, P. J.; Xu, W. J.; Qiao, S. C.; Wu, C. Q.; Liu, H. J.; Liu, D. B. et al. Synergic reaction kinetics over adjacent ruthenium sites for superb hydrogen generation in alkaline media. *Adv. Mater.* **2022**, *34*, 2110604.
[195] Zhang, Y. Q.; Liu, H. W.; Zhao, S. Y.; Xie, C.; Huang, Z. G.; Wang, S. Y. Insights into the dynamic evolution of defects in electrocatalysts. *Adv. Mater.* **2023**, *35*, 2209680.
[196] Xiao, Z. H.; Huang, Y. C.; Dong, C. L.; Xie, C.; Liu, Z. J.; Du, S. Q.; Chen, W.; Yan, D. F.; Tao, L.; Shu, Z. W. et al. *Operando* identification of the dynamic behavior of oxygen vacancy-rich Co_3O_4 for oxygen evolution reaction. *J. Am. Chem. Soc.* **2020**, *142*, 12087–12095.
[197] Wang, X.; Wu, J.; Zhang, Y. W.; Sun, Y.; Ma, K. K.; Xie, Y.; Zheng, W. H.; Tian, Z.; Kang, Z.; Zhang, Y. Vacancy defects in 2D transition metal dichalcogenide electrocatalysts: From aggregated to atomic configuration. *Adv. Mater.* **2023**, *35*, 2206576.
[198] Li, W.; Wang, D. D.; Zhang, Y. Q.; Tao, L.; Wang, T. H.; Zou, Y. Q.; Wang, Y. Y.; Chen, R.; Wang, S. Y. Defect engineering for fuel-cell electrocatalysts. *Adv. Mater.* **2020**, *32*, 1907879.
[199] Zhu, B. J.; Liang, Z. B.; Zou, R. Q. Designing advanced catalysts for energy conversion based on urea oxidation reaction. *Small* **2020**, *16*, 1906133.
[200] Yi, H.; Liu, S. Y.; Lai, C.; Zeng, G. M.; Li, M. F.; Liu, X. G.; Li, B. S.; Huo, X. Q.; Qin, L.; Li, L. et al. Recent advance of transition-metal-based layered double hydroxide nanosheets: Synthesis, properties, modification, and electrocatalytic applications. *Adv. Energy Mater.* **2021**, *11*, 2002863.
[201] Xu, H. D.; Yang, J.; Ge, R. Y.; Zhang, J. J.; Li, Y.; Zhu, M. Y.; Dai, L. M.; Li, S. A.; Li, W. X. Carbon-based bifunctional electrocatalysts for oxygen reduction and oxygen evolution reactions: Optimization strategies and mechanistic analysis. *J. Energy Chem.* **2022**, *71*, 234–265.
[202] Han, J. Y.; Guan, J. Q. Multicomponent transition metal oxides and (oxy)hydroxides for oxygen evolution. *Nano Res.* **2023**, *16*, 1913–1966.
[203] Maiti, S.; Maiti, K.; Curnan, M. T.; Kim, K.; Noh, K. J.; Han, J. W. Engineering electrocatalyst nanosurfaces to enrich the activity by inducing lattice strain. *Energy Environ. Sci.* **2021**, *14*, 3717–3756.
[204] Niu, S. W.; Fang, Y. Y.; Rao, D. W.; Liang, G. J.; Li, S. Y.; Cai, J. Y.; Liu, B.; Li, J. M.; Wang, G. M. Reversing the nucleophilicity of active sites in CoP_2 enables exceptional hydrogen evolution catalysis. *Small* **2022**, *18*, 2106870.
[205] Jin, J.; Han, X.; Fang, Y. Y.; Zhang, Z. D.; Li, Y. P.; Zhang, T. Y.; Han, A. J.; Liu, J. F. Microenvironment engineering of Ru single-atom catalysts by regulating the cation vacancies in NiFe-layered double hydroxides. *Adv. Funct. Mater.* **2022**, *32*, 2109218.
[206] Xie, Q. X.; Cai, Z.; Li, P. S.; Zhou, D. J.; Bi, Y. M.; Xiong, X. Y.; Hu, E. Y.; Li, Y. P.; Kuang, Y.; Sun, X. M. Layered double hydroxides with atomic-scale defects for superior electrocatalysis. *Nano Res.* **2018**, *11*, 4524–4534.
[207] Huang, K.; Peng, D. D.; Yao, Z. X.; Xia, J. Y.; Zhang, B. W.; Liu, H.; Chen, Z. B.; Wu, F.; Wu, J. S.; Huang, Y. Z. Cathodic plasma driven self-assembly of HEAs dendrites by pure single FCC FeCoNiMnCu nanoparticles as high efficient electrocatalysts for OER. *Chem. Eng. J.* **2021**, *425*, 131533.
[208] Liu, Y.; Li, X.; Zhang, Q. H.; Li, W. D.; Xie, Y.; Liu, H. Y.; Shang, L.; Liu, Z. Y.; Chen, Z. M.; Gu, L. et al. A general route to prepare low-ruthenium-content bimetallic electrocatalysts for pH-universal hydrogen evolution reaction by using carbon quantum dots. *Angew. Chem., Int. Ed.* **2020**, *59*, 1718–1726.
[209] Ginting, R. T.; Ovhal, M. M.; Kang, J. W. A novel design of hybrid transparent electrodes for high performance and ultra-flexible bifunctional electrochromic-supercapacitors. *Nano Energy* **2018**, *53*, 650–657.
[210] Li, F.; Han, G. F.; Noh, H. J.; Ahmad, I.; Jeon, I. Y.; Baek, J. B. Mechanochemically assisted synthesis of a Ru catalyst for hydrogen evolution with performance superior to Pt in both acidic and alkaline media. *Adv. Mater.* **2018**, *30*, 1803676.
[211] Lagadec, M. F.; Grimaud, A. Water electrolysers with closed and open electrochemical systems. *Nat. Mater.* **2020**, *19*, 1140–1150.
[212] Mu, X. Q.; Gu, X. Y.; Dai, S. P.; Chen, J. B.; Cui, Y. J.; Chen, Q.; Yu, M.; Chen, C. Y.; Liu, S. L.; Mu, S. C. Breaking the symmetry of single-atom catalysts enables an extremely low energy barrier and high stability for large-current-density water splitting. *Energy Environ. Sci.* **2022**, *15*, 4048–4057.
[213] Chen, P. Z.; Hu, X. L. High-efficiency anion exchange membrane water electrolysis employing non-noble metal catalysts. *Adv. Energy Mater.* **2020**, *10*, 2002285.
[214] Yang, J. R.; Zhu, C. X.; Li, W. H.; Zheng, X. S.; Wang, D. S. Organocatalyst supported by a single-atom support accelerates both electrodes used in the chlor-alkali industry via modification of non-covalent interactions. *Angew. Chem., Int. Ed.* **2024**, *63*, e202314382.
[215] Dresp, S.; Dionigi, F.; Loos, S.; Ferreira de Araujo, J.; Spöri, C.;

Gliech, M.; Dau, H.; Strasser, P. Direct electrolytic splitting of seawater: Activity, selectivity, degradation, and recovery studied from the molecular catalyst structure to the electrolyzer cell level. *Adv. Energy Mater.* **2018**, *8*, 1800338.

[216] Guo, L. L.; Chi, J. Q.; Zhu, J. W.; Cui, T.; Lai, J. P.; Wang, L. Dual-doping $NiMoO_4$ with multi-channel structure enable urea-assisted energy-saving H_2 production at large current density in alkaline seawater. *Appl. Catal. B: Environ.* **2023**, *320*, 121977.

[217] Dresp, S.; Dionigi, F.; Klingenhof, M.; Strasser, P. Direct electrolytic splitting of seawater: Opportunities and challenges. *ACS Energy Lett.* **2019**, *4*, 933–942.

[218] Zhong, M. X.; Xu, M. J.; Ren, S. Y.; Li, W. M.; Wang, C.; Gao, M. B.; Lu, X. F. Modulating the electronic structure of $Ni(OH)_2$ by coupling with low-content Pt for boosting the urea oxidation reaction enables significantly promoted energy-saving hydrogen production. *Energy Environ. Sci.* **2024**, *17*, 1984–1996.

[219] Qian, G. F.; Chen, J. L.; Jiang, W. J.; Yu, T. Q.; Tan, K. X.; Yin, S. B. Strong electronic coupling of CoNi and N-doped-carbon for efficient urea-assisted H_2 production at a large current density. *Carbon Energy* **2023**, *5*, e368.

[220] Xie, H.; Feng, Y. F.; He, X. Y.; Zhu, Y.; Li, Z. Y.; Liu, H. H.; Zeng, S. Y.; Qian, Q. Z.; Zhang, G. Q. Construction of nitrogen-doped biphasic transition-metal sulfide nanosheet electrode for energy-efficient hydrogen production via urea electrolysis. *Small* **2023**, *19*, 2207425.

[221] Liang, J.; Cai, Z. W.; Li, Z. X.; Yao, Y. C.; Luo, Y. S.; Sun, S. J.; Zheng, D. D.; Liu, Q.; Sun, X. P.; Tang, B. Efficient bubble/precipitate traffic enables stable seawater reduction electrocatalysis at industrial-level current densities. *Nat. Commun.* **2024**, *15*, 2950.

[222] Chen, Y.; Liu, Y. D.; Zhai, W. F.; Liu, H.; Sakthivel, T.; Guo, S. W.; Dai, Z. F. Metastabilizing the ruthenium clusters by interfacial oxygen vacancies for boosted water splitting electrocatalysis. *Adv. Energy Mater.* **2024**, *14*, 2400059.

[223] Lu, X. Y.; Pan, J.; Lovell, E.; Tan, T. H.; Ng, Y. H.; Amal, R. A sea-change: Manganese doped nickel/nickel oxide electrocatalysts for hydrogen generation from seawater. *Energy Environ. Sci.* **2018**, *11*, 1898–1910.

[224] Tong, W. M.; Forster, M.; Dionigi, F.; Dresp, S.; Sadeghi Erami, R.; Strasser, P.; Cowan, A. J.; Farràs, P. Electrolysis of low-grade and saline surface waters. *Nat. Energy* **2020**, *5*, 367–377.

[225] Ma, Y. Y.; Wu, C. X.; Feng, X. J.; Tan, H. Q.; Yan, L. K.; Liu, Y.; Kang, Z. H.; Wang, E. B.; Li, Y. G. Highly efficient hydrogen evolution from seawater by a low-cost and stable CoMoP@C electrocatalyst superior to Pt/C. *Energy Environ. Sci.* **2017**, *10*, 788–798.

[226] Luo, F.; Pan, S. Y.; Xie, Y. H.; Li, C.; Yu, Y. J.; Bao, H. F.; Yang, Z. H. Hydrazine-assisted acidic water splitting driven by iridium single atoms. *Adv. Sci.* **2023**, *10*, 2305058.

[227] Pan, S. Y.; Li, C.; Xiong, T. T.; Xie, Y. H.; Luo, F.; Yang, Z. H. Hydrogen spillover in MoO_xRh hierarchical nanosheets boosts alkaline HER catalytic activity. *Appl. Catal. B: Environ.* **2024**, *341*, 123275.

[228] Ma, R. G.; Zhou, Y.; Chen, Y. F.; Li, P. X.; Liu, Q.; Wang, J. C. Ultrafine molybdenum carbide nanoparticles composited with carbon as a highly active hydrogen-evolution electrocatalyst. *Angew. Chem., Int. Ed.* **2015**, *54*, 14723–14727.

[229] Wang, Y.; Jiao, Y. Q.; Yan, H. J.; Yang, G. C.; Tian, C. G.; Wu, A. P.; Liu, Y.; Fu, H. G. Vanadium-incorporated CoP_2 with lattice expansion for highly efficient acidic overall water splitting. *Angew. Chem., Int. Ed.* **2022**, *61*, e202116233.

[230] Li, W. D.; Liu, Y.; Wu, M.; Feng, X. L.; Redfern, S. A. T.; Shang, Y.; Yong, X.; Feng, T. L.; Wu, K. F.; Liu, Z. Y. et al. Carbon-quantum-dots-loaded ruthenium nanoparticles as an efficient electrocatalyst for hydrogen production in alkaline media. *Adv. Mater.* **2018**, *30*, 1800676.

[231] Gao, Y.; Xue, Y. R.; Qi, L.; Xing, C. Y.; Zheng, X. C.; He, F.; Li, Y. L. Rhodium nanocrystals on porous graphdiyne for electrocatalytic hydrogen evolution from saline water. *Nat. Commun.* **2022**, *13*, 5227.

[232] Jiang, B. B.; Xiao, H.; Li, J. Y.; Tang, H. L.; Chen, H.; Deng, S. J.; Tan, Y. W.; Yu, C.; Wang, J. W.; Huang, A. J. et al. Constructing Ru–Co_2P lewis acid-base pairs to prompt hydrogen evolution reaction in alkaline seawater electrolyte. *Small* **2025**, *21*, 2406900.

[233] Wu, D. L.; Liu, B.; Li, R. D.; Chen, D.; Zeng, W. H.; Zhao, H. Y.; Yao, Y. T.; Qin, R.; Yu, J.; Chen, L. et al. Fe-regulated amorphous-crystal Ni(Fe)P_2 nanosheets coupled with Ru powerfully drive seawater splitting at large current density. *Small* **2023**, *19*, 2300030.

[234] Ying, J.; Chen, J. B.; Xiao, Y. X.; de Torresi, S. I. C.; Ozoemena, K. I.; Yang, X. Y. Recent advances in Ru-based electrocatalysts for oxygen evolution reaction. *J. Mater. Chem. A* **2023**, *11*, 1634–1650.